Published in final edited form as:

Toxicol Appl Pharmacol. 2019 February 01; 364: 29–44. doi:10.1016/j.taap.2018.12.004.

Sulforaphane enriched transcriptome of lung mitochondrial energy metabolism and provided pulmonary injury protection via Nrf2 in mice

Hye-Youn Cho[1], **Laura Miller-DeGraff**[1], **Terry Blankenship-Paris**[2], **Xuting Wang**[1], **Douglas A. Bell**[1], **Fred Lih**[3], **Leesa Deterding**[3], **Vijayalakshmi Panduri**[3], **Daniel L. Morgan**[4], **Masayuki Yamamoto**[5], **Anita J. Reddy**[6], **Paul Talalay**[7], **Steven R. Kleeberger**[1]

[1]Immunity, Inflammation, and Disease Laboratory, National Institute of Environmental Health Sciences, Research Triangle Park, NC 27709, USA

[2]Comparative Medicine Branch, National Institute of Environmental Health Sciences, Research Triangle Park, NC 27709, USA

[3]Epigenetics and Stem Cell Biology Laboratory, National Institute of Environmental Health Sciences, Research Triangle Park, NC 27709, USA

[4]National Toxicology Program, National Institute of Environmental Health Sciences, Research Triangle Park, NC 27709, USA

[5]Tohoku University Graduate School of Medicine, Sendai, Japan

[6]Respiratory Institute, Cleveland Clinic, Cleveland, OH 44106, USA

[7]Department of Pharmacology and Molecular Sciences, The Johns Hopkins University School of Medicine, MD 21205, USA

Abstract

Nrf2 is essential to antioxidant response element (ARE)-mediated host defense. Sulforaphane (SFN) is a phytochemical antioxidant known to affect multiple cellular targets including Nrf2-ARE pathway in chemoprevention. However, the role of SFN in non-malignant airway disorders remain unclear. To test if pre-activation of Nrf2-ARE signaling protects lungs from oxidant-induced acute injury, wild-type (*Nrf2*$^{+/+}$) and *Nrf2*-deficient (*Nrf2*$^{-/-}$) mice were given SFN orally or as standardized broccoli sprout extract diet (SBE) before hyperoxia or air exposure. Hyperoxia-induced pulmonary injury and oxidation indices were significantly reduced by SFN or SBE in *Nrf2*$^{+/+}$ mice but not in *Nrf2*$^{-/-}$ mice. SFN upregulated a large cluster of basal lung genes that are

Correspondence: Hye-Youn Cho, Ph.D., Immunity, Inflammation, and Disease Laboratory, National Institute of Environmental Health Sciences (NIEHS), National Institutes of Health (NIH), 111 TW Alexander Dr., Building 101, MD D-201, Research Triangle Park, NC 27709, Phone: 984-287-4088, FAX: 301-480-3977, cho2@niehs.nih.gov.

AUTHOR CONTRIBUTIONS

H.-Y.C. and S.R.K. designed the study. M.Y. provided animals. P.T. provided broccoli extracts and assisted experimental design. H.-Y.C., L.M-D, D.M., A.J.R., and T.B-P. conducted experiments. X.W. and D.B. performed bioinformatic analysis. F.L and L.D. performed HPLC-mass spectrometry. V.P. measured genomic DNA damage. H.-Y.C. wrote manuscript. S.R.K. supervised research and revised manuscript.

This article has an Online Data Supplement.

CONFLICT OF INTEREST

The authors declare that they have no conflict of interest.

involved in mitochondrial oxidative phosphorylation, energy metabolism, and cardiovascular protection only in *Nrf2*$^{+/+}$ mice. Bioinformatic analysis elucidated ARE-like motifs on these genes. Transcript abundance of the mitochondrial machinery genes remained significantly higher after hyperoxia exposure in SFN-treated *Nrf2*$^{+/+}$ mice than in SFN-treated *Nrf2*$^{-/-}$ mice. Nuclear factor-κB was suggested to be a central molecule in transcriptome networks affected by SFN. Minor improvement of hyperoxia-caused lung histopathology and neutrophilia by SFN in *Nrf2*$^{-/-}$ mice implies Nrf2-independent or alternate effector mechanisms. SFN is suggested to be as a preventive intervention in a preclinical model of acute lung injury by linking mitochondria and Nrf2. Administration of SFN alleviated acute lung injury-like pathogenesis in a Nrf2-dependent manner. Potential AREs in the SFN-inducible transcriptome for mitochondria bioenergetics provided a new insight into the downstream mechanisms of Nrf2-mediated pulmonary protection.

Keywords

lung; broccoli; hyperoxia; microarray; antioxidant response element

INTRODUCTION

NF-E2-related factor 2 (Nrf2) is a transcriptional activator of antioxidant response element (ARE)-bearing defense genes. Acute lung injury (ALI) and its severe form acute respiratory distress syndrome (ARDS) affects over 200,000 annually in the U.S. It is precipitated from various clinical disorders including pneumonia, sepsis, or major trauma, and characterized by increased lung permeability and inflammation accompanying abnormal gas exchange and variable late phase responses (Hendrickson and Matthay, 2018; Matthay and Howard, 2012; Matthay et al., 2012). In laboratory rodents, inhalation of hyperoxia (>85% oxygen) causes ALI-like pulmonary injuries including edema and neutrophilic inflammation and it has been widely used as a model of ALI. We identified *Nrf2* as a susceptibility gene in the murine model of ALI (Cho et al., 2015; Cho et al., 2002b) and multiple studies using mice genetically deficient in *Nrf2* (*Nrf2*$^{-/-}$) determined its protective role in ALI-like phenotypes (Cho and Kleeberger, 2015).

Supplemental antioxidant therapies with N-acetylcysteine (NAC) or various antioxidants have had mild or inconsistent efficacy in clinical settings of oxidative lung disorders. Recent interest has focused on isothiocyanates, bioactive phytochemical antioxidants from cruciferous vegetables, particularly sulforaphane (4-methylsulfinylbutyl isothiocyanate, SFN) present as the precursor form glucoraphanin in broccoli and cauliflower. Glucoraphanin is largely hydrolyzed into SFN by myrosinase in gut microbes or in the plant itself and metabolized through the mercapturic acid pathway (60–90%) starting with glutathione S-transferase (GST)-mediated conjugation followed by sequential cleavage into other dithiocarbamates (i.e., SFN-cysteinyl-glycine, SFN-cysteine, SFN-NAC) or is converted into erucin and its conjugates by S-oxide reduction and dehydration (Budnowski et al., 2015). Metabolites of SFN or isothiocyanate were detected in most rodent tissues, blood, bile, and urine shortly after oral or systemic administration (Budnowski et al., 2015; Yanaka et al., 2009). Relatively higher accumulation of SFN metabolites were found in the lung than in other mouse tissues (Bricker et al., 2014; Clarke et al., 2011). Metabolites were

also detected in human blood and urine after single, multiple, or long-term (8–12 weeks) doses (Dinkova-Kostova and Kostov, 2012; Egner et al., 2014; Yanaka et al., 2009).

SFN acts through nuclear factor (NF)-κB inhibition and cell cycle arrest (Kensler et al., 2013). It also binds to inhibit Kelch-like ECH-associated protein 1 (Keap1, a cytoplasmic Nrf2 inhibitor) and thus is a potent inducer of Nrf2-ARE signaling (Kensler et al., 2013). Potential therapeutic spectrum of SFN has expanded from cancer to non-malignant disorders. Dietary SFN decreased gastritis symptoms in *Helicobacter pylori* (*H. pylori*) patients (Yanaka et al., 2009). SFN treatments also reduced gluconeogenesis improving glucose control in Type 2 diabetic patients (Axelsson et al., 2017). A series of clinical intervention trials demonstrated that SFN enhanced detoxification of food- and air-borne carcinogens (Egner et al., 2014). SFN-containing juice decreased the number of nasal lavage cells after challenge with diesel exhaust particles in humans (Heber et al., 2014). Further, daily doses of SFN significantly ameliorated bronchoconstriction caused by methacholine challenge in about 60% of asthmatics who participated in a clinical trial (Brown et al., 2015). However, other reports indicate mixed or negative efficacy of sulforaphane as seen in a randomized double-blind study in which oral sulforaphane did neither induce ARE-responsive genes in airway cells nor influence on lung function and inflammatory parameters in a chronic obstructive pulmonary disease cohort (Wise et al., 2016).

The current study tested the hypothesis that SFN prevents oxidant-induced ALI-like disease in a Nrf2-dependent manner. We provided *Nrf2*-sufficient ($Nrf2^{+/+}$) and -deficient ($Nrf2^{-/-}$) mice with SFN orally or as diet rich in SFN precursor glucoraphanin (standardized broccoli sprout extract, SBE) before hyperoxia (>95% O_2) exposure to determine its effect on development of lung injury. We also profiled genome-wide transcriptome changes to provide insight into the underlying pulmonary mechanisms of SFN. Results from this study provide novel insights to the role of Nrf2-mediated molecular events on lung gene expression pathways including those for mitochondrial function. Pre-treatment effects of SFN in the hyperoxia-induced model ALI may have important clinical implications.

MATERIALS AND METHODS

Animals, pretreatment, and exposure.

Male, 6–8-week-old $Nrf2^{+/+}$ (ICR), $Nrf2^{-/-}$ (ICR.129P2-*Nfe2l2*^{tm1Mym}), glutathione peroxidase 2-deicifient ($Gpx2^{-/-}$, B6.129P2-*Gpx2*^{tm1Mym}), and NAD(P)H:quinone oxidoreductase 1-deficient ($Nqo1^{-/-}$, B6;129S-*Nqo1*^{tm1Akj}) mice produced from breeding colonies at the National Institute of Environmental Health Science (NIEHS) were used in the current study. Gender- and age-matched wild-type mice, C57BL/6J ($Gpx2^{+/+}$) and 129P3/J ($Nqo1^{+/+}$), were purchased from the Jackson Laboratory (Bar Harbor, ME). $Nrf2^{-/-}$ and $Nrf2^{+/+}$ mice were provided with modified AIN-76A (AIN) diet; other mice received NIH_31 diet. Food and water were provided *ad libitum*. A subset of $Nrf2^{+/+}$ and $Nrf2^{-/-}$ mice were fed either pulverized AIN diet or AIN diet containing lyophilized SBE (Fahey et al., 2012) (as glucoraphanin 5.83 μmol/g diet) using glass jars with mesh inserts for 14 d before inhalation exposure (average consumption 21.35 μmol in 3.66 g diet/animal/day). The SBE preparation used in the current study showed reproducible daily bioavailability of SFN (average 10–18% conversion of glucoraphanin to SFN and metabolites) as determined in

urine from healthy volunteers (Fahey et al., 2015; Fahey et al., 2012). Pulverized AIN or SBE diet was provided in glass jars feeders with mesh inserts. Other *Nrf2*$^{+/+}$ and *Nrf2*$^{-/-}$ mice received 9 μmol of pure SFN (R-SFN, LKT Laboratories, Inc., St. Paul, MN) in 100 μl PBS or vehicle (PBS) by oral gavage (100 μl) at 5, 3, and 1 d before inhalation exposure. A subset of *Nqo1*$^{+/+}$ mice were fed a diet containing 0.3% dimethyl fumarate (DMF) to induce NQO1 activity for 14 d before inhalation exposure (Begleiter et al., 2004). Mice were continuously exposed to hyperoxia (>95% O_2, 48 or 72 h) in a whole-body chamber or to room air as described previously (Cho et al., 2015). Immediately following designated exposure, mice were euthanized by sodium pentobarbital overdose (104 mg/Kg). All animal use was approved by the NIEHS Animal Care and Use Committee. See details in the online data supplement.

Bronchoalveolar lavage (BAL).

Right lungs from each mouse were lavaged *in situ* with HBSS, and cells and supernatants from BAL returns were analyzed for protein content and cell differentials as described previously (Cho et al., 2015). Colorimetric assay for lactate dehydrogenase (LDH) was performed to detect cell lysis and toxicity by determination of NADH production after addition of NAD+ to aliquots (25 μl) of BAL supernatants (Sigma, St. Louis, MO). Lipid peroxidation was also determined in aliquots of BAL (25 μl) by quantification of TBARS represented by malondialdehyde-TBA using a malondialdehyde equivalence standard curve (Cell Biolabs, Inc., San Diego, CA). Sandwich ELISA was used to detect secreted mucin 5, subtypes A and C (Muc5AC) in BAL (20 μl) using a capture antibody (sc-19603, Santa Cruz Biotechnology, Santa Cruz, CA) and a detection antibody (Clone 45M1, Thermo Scientific, Fremont, CA) following the procedures described previously (Cho et al., 2013).

Lung histopathology.

Formalin-fixed left lungs were processed for H&E and AB/PAS staining. They were immunohistologically stained with voltage-dependent anion-selective channel protein 1 (VDAC1)/porin antibody (Santa Cruz) following routine immunostaining procedures.

cDNA microarray and quantitative reverse transcription-polymerase chain reaction (*qRT-PCR*).

Total lung RNA (n = 3/group) was applied to mouse 430 2.0 arrays (Affymetrix, Inc., Santa Clara, CA) in the NIEHS Microarray Core Facility as described previously (Cho et al., 2012). Array data were analyzed statistically using GeneSpring (Agilent Technologies, Inc., Santa Clara, CA). Briefly, array raw data were filtered by lower expression percentile (at least 1 sample had values within 20% cut-off rage) and the expression levels were normalized to the mean value of the control (PBS/Air/*Nrf2*$^{+/+}$) for each gene by quantile algorithm. Various interpretations were generated for group comparisons by parameters (pretreatment, exposure, genotype). Moderate t-test (PBS vs. SFN in air/*Nrf2*$^{+/+}$ or in air/*Nrf2*$^{-/-}$, air vs. hyperoxia in PBS/*Nrf2*$^{+/+}$ or in PBS/*Nrf2*$^{-/-}$) and 2-way ANOVA followed by Student-Newman-Keuls comparison (*Nrf2*$^{+/+}$ vs. *Nrf2*$^{-/-}$ with different pre-treatment/exposure) identified differentially expressed genes ($P < 0.01$). Ingenuity Pathway Analysis (IPA, Qiagen Inc., Valencia, CA) was used to identify potential molecular mechanisms. Microarray data are deposited in Gene Expression Omnibus (accession number GSE58654)

and in the NIEHS Chemical Effects in Biological Systems (CEBS; accession number: 005–00003-0121–000-2). Aliquots of lung RNA were reverse transcribed, and cDNA was subjected to PCR with gene-specific primers and 18s ribosomal RNA primer (an internal control) using an ABI Prism 7700 Sequence Detection System (Applied Biosystems, Foster City, CA).

Protein analysis.

Lung nuclear (7–10 μg) and cytosolic protein (50–100 μg) were analyzed by routine Western blotting using specific antibodies against rodent mitochondrial oxidative phosphorylation (OXPHOS) complex (Abcam, Cambridge, MA), Nrf2 (Santa Cruz), p65 NF-κB (Santa Cruz), VDAC1/porin (Santa Cruz), phopholamban (PPLA, Santa Cruz), lamin B (Santa Cruz), and pan-actin (Santa Cruz). Scanned band intensities of Western blot images (n = 3/antibody) were quantitated by densitometry (ProteinSimple, San Jose, CA). Cytosol fractions were also analyzed for total GSH amount using a commercial kit (Cell Biolabs, Inc.) to detect NADPH/GSH reductase reaction. Briefly, glutathione reductase and NADPH were added to lung cytosol fraction to generate reduced glutathione (GSH) from its oxidized form (GSSG) in the samples, which was followed by incubation with the chromogen reacting with thiol group of GSH to produce a colored compound. Changes of absorbance at 405 nm were immediately measured by 1 min intervals for ~10 min and concentration from the slope of linear portion of each sample kinetic curve was acquired using the net slopes of GSSG standards. Binding activities of nuclear proteins (5 μg) on ARE and NF-κB motifs were determined by gel shift analysis following procedures described previously (Cho et al., 2015). Specific NF-κB binding activity was quantitated by a transcription factor ELISA (Active Motif, Carlsbed, CA). Aliquots of nuclear proteins (2.5 μg) were added to wells in a 96-well plate pre-coated with an NF-κB-binding oligonucleotide. After consecutive incubation with p65 NF-κB antibody and horseradish peroxidase (HRP)-conjugated secondary antibody, binding activity of p65 NF-κB was determined by colorimetric analysis. Cold probes (addition of extra NF-κB binding oligonucleotide) were tested for reaction specificity. Total lung homogenates in radioimmunoprecipitation assay (RIPA) buffer were prepared for Western blotting and detection of oxidized protein by ELISA (Cell Biolabs, Inc.) using an anti-dinitrophenylhydrazine antibody specific to derivatized protein carbonyl groups (Cho et al., 2013).

SFN metabolite detection in urine and sera.

Non-metabolized (unconjugated) SFN and major SFN metabolites, including SFN-GSH, SFN-cysteine, and SFN- NAC, in mouse urine and sera were analyzed by HPLC-mass spectrometry. Briefly, an aliquot (10 μl) of urine was diluted with 90 μl 5% methanol and 0.1% formic acid. The sample was centrifuged at 8° C and 80 μl of supernatant was transferred to an autosampler vial containing a low volume insert. An aliquot (30 μl) of serum was diluted with 270 μl of 0.1% formic acid and loaded onto Oasis HLB solid phase extraction cartridges. Cartridges were then washed with 1 mL of 0.1% formic acid, dried with a stream of nitrogen, and eluted with 2 mL of 9:1 acetonitrile:methanol containing 0.1% formic acid. Serum eluents were dried under vacuum and reconstituted in 50 μl of 5% methanol and 0.1% formic acid solution. The prepared sample (10 μl) was injected onto an ACE Excel 3 CN-ES 2.1 X 100 mm HPLC column with gradient separation at a flow rate of

250 μl/min. Electrospray ionization and selected reaction monitoring mass spectrometry were used for analyte quantitation.

Mitochondrial genome copy number.

Mitochondrial genome copy number was determined using droplet digital PCR (ddPCR) by amplification of a short mitochondria genome fragment at NADH dehydrogenase 6, mitochondrial (*mt-Nd6*) locus (13731–13831 bp). Briefly, total lung DNA (2 ng) in PCR mixture containing SYBR Green dye and 125 nM of primers (5'-ctcccaaaccatcaagattaattac-3', 5'-gacttggggatctaactgattaatt-3') were partitioned into approximately 20,000 individual nanoliter-sized water-in-oil droplets by Bio-Rad QX200 Automated Droplet Generator (Hercules, PA) followed by PCR reaction (C1000 Touch Thermal Cycler, Bio-Rad). The droplets were then read individually in QX200 Droplet Reader (Bio-Rad) and assigned as positive (1) or negative (0). The mitochondrial copy number calculated by the positive droplets was normalized to nuclear DNA copy number determined similarly by ddPCR (primers used for beta-globin locus 54021–54122: 5'-ttctgctcaaccttcctatcag-3', 5'-ccaaactctagtcaacactcac-3').

Bioinformatic search of potential ARE.

Potential ARE sequences for Nrf2 binding were determined in selected SFN-responsive genes (n = 193) involved in mitochondrial energy production and metabolism using a position weight matrix (PWM) statistical model (Cho et al., 2012).

Statistics.

Data are expressed as group mean ± standard error (SE). Two-way ANOVA followed by Student-Newman-Keuls test for *a posteriori* comparisons to evaluate the effect of genotype ($Nrf2^{+/+}$ vs $Nrf2^{-/-}$) and treatment (AIN/air vs SFN/Air vs AIN/hyperoxia vs SFN/hyperoxia) on lung injury phenotypes and molecular analyses ($P < 0.05$). BAL phenotype data from $Nqo1^{-/-}$ and $Gpx2^{-/-}$ mouse studies were also analyzed by two-way ANOVA followed by Fisher LSD Method for *a posteriori* comparisons ($P < 0.05$).

RESULTS

Nrf2-dependent acute lung injury prevention by dietary SFN

Consistent with our previous results (Cho et al., 2002a), $Nrf2^{-/-}$ mice developed severe hyperoxic lung injury compared to $Nrf2^{+/+}$ mice after 48 h of continuous O_2 exposure (Figs. 1–3). The SBE preparation used in the current study showed reproducible bioavailability of SFN (average 10–18% conversion of glucoraphanin to SFN and metabolites) in humans (Fahey et al., 2015; Fahey et al., 2012), and has been applied to various clinical studies (Egner et al., 2014; Heber et al., 2014; Kensler et al., 2012). Average glucoraphanin consumption was 21.35 μmol in 3.66g SBE diet/animal/day, which was equivalent to about 6 g of mature broccoli or 0.9 g broccoli sprouts (Fahey et al., 1997). Compared to control (AIN) diet, 14-day SBE diet significantly lowered hyperoxia exposure-induced lung neutrophil number and protein concentration in $Nrf2^{+/+}$ mice (Fig. 1A) as assessed by BAL analysis. However, no significant diet effects were found on lung phenotypes in $Nrf2^{-/-}$ mice after hyperoxia (Fig.1A, note the differences in y-axis scales for $Nrf2^{+/+}$ and $Nrf2^{-/-}$).

Lung LDH concentration, a marker of cell lysis, was increased by hyperoxia and SBE significantly reduced this effect *Nrf2*$^{+/+}$ mice (Fig. 1B). Compared to AIN, SBE significantly inhibited body weight loss caused by hyperoxia in *Nrf2*$^{+/+}$ mice, but not in *Nrf2*$^{-/-}$ mice (Fig. 1C). AIN and SBE had no effect on lung histopathology in air-exposed mice (Fig. 2). Hyperoxia-induced key histopathologic changes (e.g., perivascular-peribronchial edema, inflammatory cell infiltration, mucous hypersecretion) in *Nrf2*$^{+/+}$ mice were reduced by SBE pre-treatment compared to those with AIN (Fig. 2). Severe histopathologic phenotypes in *Nrf2*$^{-/-}$ mice by hyperoxia were only marginally improved by SBE compared to AIN (Fig. 2).

Nrf2-dependent acute lung injury prevention by oral SFN

Oral administration of pure SFN (9 μmol/animal at 5-, 3-, and 1-day before start of inhalation exposure) significantly reduced BAL neutrophil and epithelial cell numbers as well as mucus hypersecretion (determined by measurement of Muc5AC) in hyperoxia-exposed *Nrf2*$^{+/+}$ mice (Fig. 3A). The SFN dose was determined based on bioavailability of SFN metabolites in murine lungs reported in previous studies (Clarke et al., 2011). Hyperoxia-increased BAL neutrophils in *Nrf2*$^{-/-}$ mice were significantly lowered by SFN pretreatment, but no SFN effect was found in hyperoxia-induced lung cell death and mucus hypersecretion in these mice (Fig. 3A). Relative to vehicle (PBS), SFN significantly lowered the magnitude of hyperoxia-increased lung protein oxidation (determined by protein carbonyl) and lipid peroxidation (determined by thiobarbituric acid reactive substance, TBARS) in *Nrf2*$^{+/+}$ mice, but not in *Nrf2*$^{-/-}$ mice (Fig. 3B). Total lung glutathione level (reduced GSH form) was also significantly elevated by SFN in *Nrf2*$^{+/+}$ mice after hyperoxia (Fig. 3B). Although SFN increased basal GSH level in *Nrf2*$^{-/-}$ lungs, the overall GSH pool was significantly lower after air or hyperoxia in *Nrf2*$^{-/-}$ mice compared to *Nrf2*$^{+/+}$ mice (Fig. 3B).

SFN and metabolites were detected in mouse sera and urine until 3–4 days after the last oral SFN administration (Fig. 3C). In urine, primary metabolites were SFN-cysteine and SFN-NAC while the unconjugated SFN and SFN-GSH levels were negligible. Less than 1 pg/μl of unconjugated SFN, SFN-GSH, and SFN-NAC was detected but not SFN-cysteine in sera. No genotype or exposure effects were found on metabolite levels or composition.

Nrf2-dependent lung transcriptomics

1. **SFN effects on air control mice—**Supplemental SFN significantly altered the basal lung transcriptome in air-exposed *Nrf2*$^{+/+}$ mice (n = 1,187, $P < 0.01$). Hierarchical clustering indicated these genes responded to SFN in *Nrf2*$^{+/+}$ but not in *Nrf2*$^{-/-}$ mice (Fig. 4A). Transcripts were highly enriched for mitochondrial functions, OXPHOS, TCA cycle, substrate carriers and transporters, and biogenesis (Figs. 4B–C, Tables 1 and E1). Genes including NADH dehydrogenases (e.g., *Ndufs1*), cytochrome c oxidases (e.g., *Cox7a1*), isocitrate dehydrogenase 3 (NAD+) alpha (*Idh3a*), ATP synthases (e.g., *Atp5g1*), peroxisome proliferator activated receptor, gamma, coactivators (e.g., *Ppargc1a*), aconitase 2, mitochondrial (*Aco2*), and mitochondrial symporters (e.g., *Mpc1*) were largely upregulated (≤ 4-fold). In addition to nuclear-encoded mitochondria genes, SFN induced (≤ 32-fold) genes related to mitochondrial energy metabolism (Figs. 4B and 4D, Tables 1 and

E1) including lipid-carbohydrate-amino acid catabolism (e.g., *Adipoq*, *Fabp4*, *Acadl*, *Slc2a4*) and cardiovascular-muscular contractility and calcium homeostasis including natriuretic peptide type A (*Nppa*), phopholamban (*Pln*), corin (*Corin*), and myosins (e.g., *Myl3*). SFN also significantly increased many antioxidant (e.g., *Ephx2*, *Car3*) and immunity genes (e.g., *Ltf*, *Muc5b*) in $Nrf2^{+/+}$ mice (Tables 1 and E1). In contrast, SFN significantly decreased genes encoding tissue injury (e.g., Tnf receptor-associated factor 1, *Traf1*), oxidant production (e.g., NADPH oxidase 4, *Nox4*) and downstream targets of vitamin D3 receptor/retinoid X receptor (RXR) signaling in $Nrf2^{+/+}$ lungs, and multiple mitogen-activated protein kinase (MAPK) cascade enzymes (e.g., *Map3k8*) and NF-κB were predicted to play central roles in their networks (Table E1, Fig. 4E).

In $Nrf2^{-/-}$ lungs, SFN-modulated genes (n = 250, $P < 0.01$) were involved in inflammation and organismal injury pathways (Table E2). Chemokine (C-C motif) ligand 11 (*Ccl11*), *Ccl20*, and sorbitol dehydrogenase (*Sord*) are examples of genes affected by SFN only in $Nrf2^{-/-}$ mice. A limited number (n = 17) of genes (e.g., *Myoz2*, *Gsto1*) were modulated commonly by SFN in both genotypes, which indicates that SFN differentially influenced some pulmonary transcriptomics independent of *Nrf2*.

Selected SFN-induced genes related to mitochondria, energy metabolism, and cardiovascular function (n = 193) have multiple ARE-like motifs (PWM score of ≥ 6.4) for Nrf2 binding (Tables 1, E3). Some potential AREs have been functionally verified by chromatin immunoprecipitation followed by DNA sequencing (Mouse et al., 2012; Yue et al., 2014), supporting roles as Nrf2 downstream effectors.

2. Hyperoxia effects—As we previously reported (Cho et al., 2005), hyperoxia significantly altered lung transcriptomics in $Nrf2^{+/+}$ mice (n = 7,162, $P < 0.01$). Pathway analyses suggested that p53, together with PDGF, coagulation factor 2 (F2), TNF, and Nrf2 were key upstream regulators for transcriptome changes by O_2 (Fig. 5A, Table E4). A role for p53 in this ALI model is explained by its functions in anti-oxidant induction, mitochondrial energy metabolism, and co-regulation with the Keap1-Nrf2 pathway and DNA damage response (Bensaad and Vousden, 2007). During the development of hyperoxic lung injury, genes involved in extracellular matrix degradation [e.g., matrix metalloproteinase 3 (*Mmp3*), heparin-binding EGF-like growth factor (*Hbegf*)] and smooth muscle cell migration in response to vascular injury (as suggested by increased gene transcripts such as plasminogen activator, urokinase receptor, *Plaur*) may be activated by MAPKs, IL-1, or PDGF. Nrf2-mediated oxidative responses by well-known ARE-bearing antioxidants as well as Nrf2-dimerizing transcription factors (e.g., *Mafk*), protein ubiquitination and proteasomal degradation (e.g., ubiquitin-conjugating enzyme E2K, *Ube2k*), and phase 3 transporters (e.g., *Apcc1*) were the most affected pathways during hyperoxia exposure (Table E4), further supporting *Nrf2* as an important susceptibility gene in this model. Hyperoxia also upregulated multiple amino acyl tRNA synthetases (e.g., seryl-tRNA synthetase, *Sars*) for tRNA charging and integrin linked kinase (ILK) signaling in $Nrf2^{+/+}$ mice (Table E4). Coordinated transcriptional induction of sequestrome 1 (*Sqstrm1*) with vacuolar proton pumps (e.g., ATPase, H+ transporting, lysosomal such as *Atp6v0a1*), cathepsins (e.g., *Ctsh*), and vacuolar protein sorting proteins (e.g., *Vps8*)

suggested lysosomal degradative function and autophagy was also triggered by hyperoxia in *Nrf2*$^{+/+}$ mice (Perera et al., 2015).

In *Nrf2*$^{-/-}$ lungs, hyperoxia-induced transcriptome changes (n = 4,799, $P < 0.01$) were associated with acute and acquired immune responses and immune cell trafficking [e.g., serum amyloid A 3 (*Saa3*), *Il6*, *Ccl7*, *Mmp3*], and IL-17α, TNF, IL-1, NF-κB, and toll like receptors (TLRs) were suggested as upstream regulators of the hyperoxia-response genes in *Nrf2*$^{-/-}$ lungs (Fig. 5B, Table E5). Many of these hyperoxia-responsive genes in *Nrf2*$^{-/-}$ lungs were not affected in *Nrf2*$^{+/+}$ lungs. Similar pathways were demonstrated by Nrf2-dependently altered genes during hyperoxia (n = 816, $P < 0.01$, Table E6). Overall analyses indicated that immune and inflammatory signaling through IL-17α and pattern recognition receptor-mediated signaling on downstream genes including selectin, platelet (*Selp*), CD14 antigen (*Cd14*), *Ccl7*, and Fc receptor, IgG, l low affinity IIb (*Fcgr2b*) correlate with more severe lung injury including protein edema in *Nrf2*$^{-/-}$ mice relative to *Nrf2*$^{+/+}$ mice (Figs. 5C and 6A-top panel, Table E6).

3. SFN and hyperoxia effects—In *Nrf2*$^{+/+}$ mice, SFN pretreatment significantly altered 264 lung genes ($P < 0.01$, 2-Way ANOVA, Table E7) during ALI-like phenotype development by hyperoxia. IPA indicated that they were involved in protein post-translational modification (e.g., *Ube2d3*), vascular-endothelial development (e.g., *Ddah1*, *Cdc16*), and phospholipid signaling/metabolism (e.g., *S1pr1*), suggesting that SFN predisposed to regulatory protein degradation, cell membrane signaling, and endothelial integrity to counter pulmonary hyperoxia toxicity.

Comparative analysis between *Nrf2*$^{+/+}$ and *Nrf2*$^{-/-}$ mice identified Nrf2-dependently changed genes by SFN during hyperoxia (n = 1,007, $P < 0.01$). Most of the mitochondrial function and energy metabolism genes (e.g., *Ndufs1*, *Atp5b*, *Idh2*, *Acadl, Slc25a17*, *Dnaja3*) remained consistently higher in SFN-treated *Nrf2*$^{+/+}$ than in SFN-treated *Nrf2*$^{-/-}$ in response to hyperoxia (Table E8, Fig. 6A). This suggests their roles in SFN-Nrf2-mediated lung protection against hyperoxia. Genes encoding NF-κB (e.g., *Traf3*, *Casp8*) and PPAR/RXR (e.g., *Il1r1*, *Nr2f1*) signal transducers were also Nrf2-dependently expressed in SFN-treated lungs during hyperoxia (Table E8, Fig. 6A-bottom graph), which indicated that SFN inhibited lung inflammatory response in a Nrf2-dependent manner for lung protection. In addition, SFN heightened the expression of cancer (e.g., *Fgfr1*, *Kit*, *Pdgfrb*) and immunity (e.g., *Prg4*, *Itga9)* genes but suppressed metabolic antioxidant genes (e.g., *Ces1g*, *Got1*, *Akr1b7*) in *Nrf2*$^{-/-}$ mice relative to *Nrf2*$^{+/+}$ mice after hyperoxia. Pearson and Spearman metric analyses (r > 0.95) clustered Nrf2-dependently modulated genes by similar expression profiles (Fig. 6B). *Corin*-like genes that were SFN-inducible in air-*Nrf2*$^{+/+}$ lungs and suppressed by hyperoxia more significantly in *Nrf2*$^{-/-}$ mice than in *Nrf2*$^{+/+}$ mice (Profile 1) were involved in cardiovascular tone and energy metabolism. Signal transducers including *Map3k8* (Profile 2) were decreased by SFN in air-exposed *Nrf2*$^{+/+}$ mice but induced by SFN in hyperoxia-*Nrf2*$^{-/-}$ mice. *Nqo1*-like genes that were upregulated by SFN and hyperoxia only in *Nrf2*$^{+/+}$ mice (Profile 3) encoded antioxidants and mitochondrial/lipid metabolism proteins. Profiles 4 and 5 included solute carrier family 7 member 11 (*Slc7a11*)- or *Selp*-like genes modulated Nrf2-dependently by hyperoxia, but not by SFN.

In *Nrf2*$^{-/-}$ mice, hyperoxia- and SFN-responsive genes (n = 533, $P < 0.01$) were dissociated from those in *Nrf2*$^{+/+}$ mice. This indicated that SFN triggered different pulmonary response mechanisms in the absence of Nrf2. Pathway analysis demonstrated that these *Nrf2*$^{-/-}$ unique genes (e.g., *Sele*, *Itga5*, *Lif*, *Flnb*) may stimulate cellular movement and interaction in hyperoxia-injured extracellular matrix and connective tissues by activating cell spreading, attachment, and homing (Fig. 6C), through which SFN may exert Nrf2-independent, mild protection against hyperoxia.

4. Validation of microarray data

Effect of SFN on mitochondrial proteins: Lung mitochondrial genome copy number determined by PCR method (Furda et al., 2014) was not significantly affected by genotype, exposure, or pretreatment (Table 2). Immunohistochemical localization of VDAC1 for mitochondrial membrane potential, a marker of mitochondrial function or biogenesis, was dense in alveolar macrophages, type 2 cells, and bronchial epithelium and smooth muscle as well as endothelium and vascular myocytes of pulmonary arteries in normal mice (PBS/Air), and little variation was found between two genotypes (Fig. 7A). In air-exposed control *Nrf2*$^{+/+}$ mice, SFN increased VDAC1-positive cells in pulmonary arteries and terminal bronchioles, but not in *Nrf2*$^{-/-}$ mice. This observation was consistent with SFN-induced transcriptional induction of vascular-muscular genes (e.g., *Nppa*, *Corin*, *Pln*, *Myl3*) and muscle-related mitochondrial genes (e.g., *Fabp3*, *Cox7a1*) in air-*Nrf2*$^{+/+}$ mice (see Fig. 4B). Hyperoxia reduced VADC1 staining in alveoli, arterial endothelium, and myocytes in both genotypes, indicating mitochondrial dysfunction or mitophagy in these cells. In contrast, hyperoxia increased VDAC1 proteins in injured small vessels (perivascular edema, hypertrophy) and hyperplastic bronchial/terminal bronchial epithelium in *Nrf2*$^{+/+}$ mice. SFN pretreatment rescued hyperoxia-induced loss of alveolar VDAC1 and enhanced VDAC-positive cells in pulmonary artery and distal airway epithelium of *Nrf2*$^{+/+}$ mice. Hyperoxia and SFN effect on VDAC1 expression was relatively marginal in *Nrf2*$^{-/-}$ mice.

Western blot analyses determined expression of OXPHOS complex, PPLA, and VDAC1 (Fig. 7B). Representative proteins from mitochondrial complexes I (NDUFB8), IV (MT-CO1 encoded by mitochondral genome), and V (ATP5A) subunits were increased by SFN and hyperoxia in *Nrf2*$^{+/+}$ mice while succinate dehydrogenase complex, subunit B (SDHB) in complex II was increased by SFN but decreased after hyperoxia in *Nrf2*$^{+/+}$ mice. SFN effects on these OXPHOS subunits were relatively marginal in *Nrf2*$^{-/-}$ mice.

Effect of SFN on redox transcription factors: Nuclear ARE binding activity and translocated Nrf2 were increased by hyperoxia exposure in *Nrf2*$^{+/+}$ mice at 3 days after hyperoxia while SFN pretreatment reduced nuclear Nrf2 level compared to PBS, probably due to the lowered oxidative stress and injury by SFN (Fig. 7C). Lung NF-κB level was determined to be a key molecule of the transcriptome networks influenced by SFN (Fig. E4A). Total NF-κB-DNA binding activity and specific p65 NF-κB activity was increased by hyperoxia in both genotypes, with higher DNA binding activity in PBS-treated *Nrf2*$^{-/-}$ mice than PBS-treated *Nrf2*$^{+/+}$ mice (Fig. 7D). SFN significantly decreased NF-κB-DNA binding activity in *Nrf2*$^{+/+}$ mice but not in *Nrf2*$^{-/-}$ mice after hyperoxia, indicating Nrf2-dependent SFN inhibition of NF-κB activity (Fig. 7D).

Functional roles of SFN-inducible ARE antioxidant enzymes: ARE-bearing *Nqo1* and *Gpx2* were among downstream antioxidant enzymes elevated by both hyperoxia and SFN. Hyperoxia-induced increase in lung BAL neutrophils was significantly greater (48–72 h) in $Nqo1^{-/-}$ mice and significantly lower (72 h) in mice fed with NQO1-inducing DMF diet ($Nqo1^{+/+}DMF$), compared to $Nqo1^{+/+}$ mice (Fig. 8A). Numbers of BAL epithelial cells were significantly increased by hyperoxia (48–72 h) in $Nqo1^{-/-}$ mice, but not in $Nqo1^{+/+}$ and $Nqo1^{+/+}DMF$ mice (Fig. 8A). BAL neutrophil (48 h) and epithelial cell (48–72 h) numbers were significantly higher in $Gpx2^{-/-}$ mice than in $Gpx2^{+/+}$ mice after hyperoxia (Fig. 8B).

DISCUSSION

We report in the current study that antioxidant SFN decreased susceptibility of mouse lungs to oxidant-induced ALI, and Nrf2 contributed to SFN-mediated protection. Genome-wide transcriptome analysis suggested that SFN may supplement substrates for mitochondrial function and energy metabolism in an Nrf2-dependent manner to enable the lung to reduce oxidant injury while *Nrf2*-deficiency may limit metabolic substrates and thus impair the mitochondria-mediated cellular processes. Our novel findings *in vivo* demonstrated prevention of ALI-like disorder by SFN that may have important clinical implications and provided molecular aspects of pulmonary SFN action.

Genetic polymorphisms in *GSTM1* and *GSTT1*, which are Nrf2-inducible enzymes that convert SFN into SFN-GSH, affected SFN excretion and plasma levels as well as excretion of xenobiotic conjugates in humans who took SFN-rich dietary supplement (Egner et al., 2014; Gasper et al., 2005). This indicated correlation of NRF2 with bioavailability and efficacy of SFN. SFN efficacy has been widely investigated in murine models of various disorders (Dinkova-Kostova and Kostov, 2012), and Nrf2-dependent roles of SFN, particularly in inflammatory and infectious airway diseases, were reported using $Nrf2^{+/+}$ and $Nrf2^{-/-}$ mice. Inhaled arsenic-induced lung injury was Nrf2-dependently inhibited by SFN (Zheng et al., 2012). We previously reported that orally administered SFN significantly lowered respiratory syncytial virus load and lung inflammation in $Nrf2^{+/+}$ but not in $Nrf2^{-/-}$ mice (Cho et al., 2009). SFN also decreased bacterial growth on co-cultured alveolar macrophages isolated from chronic obstructive pulmonary disorder patients and inhibition of an Nrf2-regulated scavenger receptor decreased the phagocytic effects of SFN (Harvey et al., 2011). Airway hyperresponsiveness and inflammation by chlorine gas was also resolved by sulforaphane in $Nrf2^{+/+}$ mice but not in $Nrf2^{-/-}$ mice (Ano et al., 2017). In a ovalbumin and cigarette smoke model of refractory asthma, sulforaphane restored steroid therapy sensitivity through activation of histone deacetylase 2 in an Nrf2-dependent manner (Sakurai et al., 2018).

Importantly, we determined that SFN markedly increased transcription of genes involved in mitochondrial respiration and energy metabolism and cardiovascular-muscle function in $Nrf2^{+/+}$ lungs, but not in $Nrf2^{-/-}$ lungs. Transcription of mitochondrial OXPHOS complex, transporters/symporters, and TCA cycle enzymes was coordinately increased with transcription of enzymes in fatty acid β-oxidation (FAO), glycolysis, and amino acid degradation pathways which provide the OXPHOS chain with metabolic substrates and electrons (Fig. 9). SFN-mediated induction of the transcriptome for mitochondria and

metabolism was manifest basally and expression of these genes was consistently greater in *Nrf2*$^{+/+}$ lungs than in *Nrf2*$^{-/-}$ lungs after hyperoxia. Hyperoxia may cause cell- or region-specific changes in mitochondrial function and energy metabolism as predicted by focal changes of VDAC1 in *Nrf2*$^{+/+}$ lungs. SFN also induced transcripts in mitochondrial biogenesis and homeostasis, *Ppargc1a* and *Ppargc1b* for mitochondrial reactive oxygen species (ROS) removal/metabolism and *Mfn2* and *Mtfp1* for mitochondrial fusion/fission. Overall, we postulate that SFN fortifies mitochondrial functions to protect lungs against oxidative insult. Recent studies have underscored a role for Nrf2 in induction of genes for FAO, NADPH generation, ATP synthesis, and mitophagy (Tebay et al., 2015). Nrf2 also increased mitochondrial biogenesis and autophagy in rodent lung and other tissues under stressed conditions via induction of heme oxygenase-1, superoxide dismutase 2 (SOD2), and PGC-1α (Chang et al., 2015). In animal models with high glucose availability or in cancer cells, Nrf2 redirected glucose metabolism from aerobic pyruvate/TCA cycle into anabolic pentose-phosphate pathway (Chartoumpekis et al., 2015).

Mitochondria DNA copy number is known to vary constantly depending on energy demands (Clay Montier et al., 2009). Different from genomic DNA, the mitochondrial genome is vulnerable to ROS damage probably in part due to the lack of histone protection and effective DNA repair mechanisms (Tatarenkov and Avise, 2007), and the copy number of mitochondrial DNA may be altered by damage, resulting in mitochondrial dysfunction. It has been therefore considered as a critical component of overall mitochondrial health, and has been related to aging and disease conditions such as cancer, cardiovascular diseases, neurodegenerative disorders, and infertility (Ashar et al., 2017; Yue et al., 2018). We did not find significant changes in pulmonary mitochondrial genome by hyperoxia or SFN at 3 days of hyperoxia exposure. Therefore, SFN action on mitochondria in the current system may be mainly through transcriptional activation of genomic DNA-encoded mitochondrial proteins. While Nrf2 and hyperoxia effects on mitochondrial DNA was not significant at the current time-frame of the experiments, further studies are warranted at early period of lung injury development by hyperoxia

Functional roles of Nrf2 in mitochondrial metabolism have been strongly supported in mice with altered *Nrf2* expression (i.e., *Nrf2*-deficient, *Keap1*-knockdown). Proteomics approaches found differential hepatic lipid metabolism and mitochondrial enzymes in *Nrf2*$^{+/+}$ and *Nrf2*$^{-/-}$ mice, and potential AREs were elucidated in *Vdac1*, ornithine aminotransferase (*Oat*), and *Atp5a1* (Abdullah et al., 2012). *Nrf2*-deficiency lowered basal mitochondrial membrane potential and suppressed O_2 consumption, FAO, and OXPHOS in various tissues and cells (Ludtmann et al., 2014). Augmented mitochondrial functions and upregulation of FAO genes were found in *Keap1*-knockdown mice after caloric restriction (Kulkarni et al., 2013; Ludtmann et al., 2014). Mitochondrial morphology and integrity change by H_2O_2 in rat cardiomyocytes were *Nrf2*-dependently preserved (Strom et al., 2016). Enhanced mitochondrial and total ROS production were apparent in *Nrf2*-deficient cortical slice and glio-neuronal co-culture, and the authors attributed these changes to the limited substrates and impaired activity of complex I in *Nrf2*$^{-/-}$ systems (Kovac et al., 2015). *Nrf2*-deficient neurons also had altered NADH and flavin adenine dinucleotide homeostasis coupled with reduced ATP production (Holmstrom et al., 2013). Nrf2-mediated mitochondrial quality control (copy number increase, mitophagy and biogenesis gene

induction) was also linked with resolution of lung bacterial inflammation (Athale et al., 2012; Chang et al., 2015).

Mitochondria sense intracellular Ca^{2+} concentration for homeostasis, which is particularly critical in metabolically active myocardium and airway/vascular smooth muscles. Mitochondrial dysfunction is prominent in myocardial hypertrophy or cardiomyopathy, and a null mutation in adenine nucleotide translocator-1 (*ANT1* or *SLC25A4*) was associated with the disease (Strauss et al., 2013). Mitochondrial compromise is also characteristic in pulmonary artery hypertension which is closely related to cardiac pathogenesis. Mitochondrial ROS and diffusible metabolites have been proposed to activate NLRP3 inflammasome and TLR9 leading to vascular remodeling and pulmonary hypertension (Sutendra and Michelakis, 2014). We reported that cardio-muscular Ca^{2+}-pump regulator *Pln*, blood pressure-lowering *Nppa*, and natriuretic peptide-activating *Corin* were markedly induced by SFN only in wild-type mice, suggesting Nrf2-dependent SFN action on cardiovascular tone. Supporting this concept, Strom et al. (Strom et al., 2016) found increased sensitivity of mitochondria to swelling by Ca^{2+} in $Nrf2^{-/-}$ hearts compared to $Nrf2^{+/+}$ hearts. A glucoraphanin-containing diet also ameliorated hypertension and atherosclerotic changes in spontaneously hypertensive, stroke-prone rats (Lopes et al., 2015). Taken together with potential AREs that we found in these genes, SFN may protect the cardiovascular system models through Nrf2-dependent induction of vasodilating and cardio-muscular Ca^{2+} handing genes.

In conclusion, results suggest a preventive role for SFN in development of ALI-like phenotypes in adult mice. These results may have important implications for the prevention of ALI in clinical settings where sepsis, blunt force trauma, and other disorders may lead to ALI or acute respiratory distress syndrome (e.g.(Marzec et al., 2007)). Molecular mechanisms underlying SFN action may be in part attributed to enhancing pulmonary mitochondrial integrity and dynamics thus diminishing oxidant toxicity. Differential transcriptome changes in *Nrf2*-sufficient and -deficient lungs imply that SFN action is primarily via Nrf2. NF-κB or MAPKs, central to multiple molecular networks of the Nrf2-dependently changed genes by SFN, may also be critical signal transducers in response to SFN. Our studies support the emerging concept of Nrf2-mitochondria linkage, particularly in association with potential intervention in asthma, ALI/ARDS, and chronic obstructive distress syndrome where transfer of stem cell or stem cell mitochondria to airway cells attenuated mitochondrial dysfunction and reduced pulmonary inflammation (Ahmad et al., 2014; Islam et al., 2012; Li et al., 2018; Morrison et al., 2017). While we examined effects of systemic SFN in the lung only at the peak of hyperoxic injury, additional examination of early molecular events and extra pulmonary (e.g., heart, liver) effects will add to our understanding of SFN mechanisms. Finally, it is important to note there is increasing evidence of genotoxicity (e.g., DNA mutation, DNA strand break, or DNA adduct formation) by broccoli extracts or SFN (Latte et al., 2011; Sestili et al., 2010) which warrants investigation of undesirable, off-target effects of SFN.

Supplementary Material

Refer to Web version on PubMed Central for supplementary material.

ACKNOWLEDGMENTS

This research was supported by the Intramural Research Program of the NIEHS, National Institutes of Health, Department of Health and Human Services. The authors thank. Mr. Herman Price for coordinating hyperoxia exposures at the NIEHS Inhalation Facility under contract to Alion Science and Technology, Inc. Microarray analysis was performed at the NIEHS Microarray Core, and Ms. Carolyn Favaro and Ms. Isabel Lea in the National Toxicology Program submitted array data to GEO and NIEHS CEBS. Drs. Richard S. Paules and Alison Harrill at the NIEHS provided excellent critical review of the manuscript.

LIST OF ABBREVIATIONS

Aco2	aconitase 2, mitochondrial
AIN	AIN-76A diet
ALI	acute lung injury
ANT1	adenine nucleotide translocator-1
ARDS	acute respiratory distress syndrome
ARE	antioxidant response element
Atp	ATP synthase
BAL	bronchoalveolar lavage
CCL	Chemokine (C-C motif) ligand
CEBS	Chemical Effects in Biological Systems
Cox	cytochrome c oxidase
ddPCR	droplet digital PCR
DMF	dimethyl fumarate
FAO	fatty acid β-oxidation
Gpx2	glutathione peroxidase
GSH	reduced glutathione
GSSG	oxidized glutathione
GST	glutathione-S-transferase
H. pylori	*Helicobacter pylori*
HRP	horseradish peroxidase
Idh3a	isocitrate dehydrogenase 3 (NAD+) alpha
ILK	integrin-linked kinase
IPA	Ingenuity Pathway Analysis

Keap1	Kelch-like ECH-associated protein 1
LDH	lactate dehydrogenase
MAPK	mitogen-activated protein kinase
Mmp3	matrix metalloproteinase 3
Mpc	mitochondrial symporter
Mt	mitochondria
MT-CO1	mitochondrially encoded cytochrome c oxidase subunit 1
Muc5ac	mucin 5, subtypes A and C
NAC	N-acetylcysteine
Nduf	NADH dehydrogenase (Ubiquinone)
mt-Nd6	NADH dehydrogenase 6, mitochondrial
Nox4	NADPH oxidase 4
Nppa	natriuretic peptide type A
NQO1	NAD(P)H:quinone oxidoreductase
Nrf2	NF-E2 related factor 2
100% O_2 or O_2	hyperoxia
Oat	ornithine aminotransferase
OXPHOS	oxidative phosphorylation
Pln, PPLA	phopholamban
PPAR	peroxisome proliferator activated receptor
***Ppargc1a*, PGC-1α**	peroxisome proliferator activated receptor, gamma, coactivators
PWM	position weight matrix
RIPA	radioimmunoprecipitation assay
qRT-PCR	quantitative reverse transcription-polymerase chain reaction
ROS	reactive oxygen species
RXR	retinoid X receptor
SBE	standardized broccoli sprout extract
SDHB	Succinate dehydrogenase complex, subunit B

Selp	selectin, platelet
SFN	sulforaphane
Slc7a11	solute carrier family 7 member 11
SOD	superoxide dismutase
Sord	sorbitol dehydrogenase
TBARS	thiobarbituric acid reactive substances
Tlr	toll like receptor
VDAC1	voltage-dependent anion-selective channel protein 1

REFERENCES

Abdullah A, Kitteringham NR, Jenkins RE, Goldring C, Higgins L, Yamamoto M, Hayes J, Park BK, 2012 Analysis of the role of Nrf2 in the expression of liver proteins in mice using two-dimensional gel-based proteomics. Pharmacol. Rep PR 64, 680–697. [PubMed: 22814021]

Ahmad T, Mukherjee S, Pattnaik B, Kumar M, Singh S, Kumar M, Rehman R, Tiwari BK, Jha KA, Barhanpurkar AP, et al., 2014 Miro1 regulates intercellular mitochondrial transport & enhances mesenchymal stem cell rescue efficacy. EMBO J 33, 994–1010. [PubMed: 24431222]

Ano S, Panariti A, Allard B, O'Sullivan M, McGovern TK, Hamamoto Y, Ishii Y, Yamamoto M, Powell WS, Martin JG, 2017 Inflammation and airway hyperresponsiveness after chlorine exposure are prolonged by Nrf2 deficiency in mice. Free. Radic. Biol. Med 102, 1–15. [PubMed: 27847240]

Ashar FN, Zhang Y, Longchamps RJ, Lane J, Moes A, Grove ML, Mychaleckyj JC, Taylor KD, Coresh J, Rotter JI, et al., 2017 Association of Mitochondrial DNA Copy Number With Cardiovascular Disease. JAMA Cardiol 2, 1247–1255. [PubMed: 29049454]

Athale J, Ulrich A, Chou Macgarvey N, Bartz RR, Welty-Wolf KE, Suliman HB, Piantadosi CA, 2012 Nrf2 promotes alveolar mitochondrial biogenesis and resolution of lung injury in Staphylococcus aureus pneumonia in mice. Free. Radic. Biol. Med 53, 1584–1594. [PubMed: 22940620]

Axelsson AS, Tubbs E, Mecham B, Chacko S, Nenonen HA, Tang Y, Fahey JW, Derry JMJ, Wollheim CB, Wierup N, et al., 2017 Sulforaphane reduces hepatic glucose production and improves glucose control in patients with type 2 diabetes. Sci. Transl. Med 9, eaah4477. [PubMed: 28615356]

Begleiter A, Leith MK, Thliveris JA, Digby T, 2004 Dietary induction of NQO1 increases the antitumour activity of mitomycin C in human colon tumours in vivo. Br. J. Cancer 91, 1624–1631. [PubMed: 15467770]

Bensaad K, Vousden KH, 2007 p53: new roles in metabolism. Trends. Cell. Biol 17, 286–291. [PubMed: 17481900]

Bricker GV, Riedl KM, Ralston RA, Tober KL, Oberyszyn TM, Schwartz SJ, 2014 Isothiocyanate metabolism, distribution, and interconversion in mice following consumption of thermally processed broccoli sprouts or purified sulforaphane. Mol. Nutr. Food. Res 58, 1991–2000. [PubMed: 24975513]

Brown RH, Reynolds C, Brooker A, Talalay P, Fahey JW, 2015 Sulforaphane improves the bronchoprotective response in asthmatics through Nrf2-mediated gene pathways. Respir. Res 16, 106. [PubMed: 26369337]

Budnowski J, Hanske L, Schumacher F, Glatt H, Platz S, Rohn S, Blaut M, 2015 Glucosinolates Are Mainly Absorbed Intact in Germfree and Human Microbiota-Associated Mice. J. Agric. Food. Chem 63, 8418–8428. [PubMed: 26365197]

Chang AL, Ulrich A, Suliman HB, Piantadosi CA, 2015 Redox regulation of mitophagy in the lung during murine Staphylococcus aureus sepsis. Free Radic. Biol. Med78, 179–189. [PubMed: 25450328]

Chartoumpekis DV, Wakabayashi N, Kensler TW, 2015 Keap1/Nrf2 pathway in the frontiers of cancer and non-cancer cell metabolism. Biochem. Soc. Trans 43, 639–644. [PubMed: 26551705]

Cho HY, Gladwell W, Yamamoto M, Kleeberger SR, 2013 Exacerbated airway toxicity of environmental oxidant ozone in mice deficient in Nrf2. Oxid. Med. Cell. Longev 2013, 254069. [PubMed: 23766849]

Cho HY, Imani F, Miller-DeGraff L, Walters D, Melendi GA, Yamamoto M, Polack FP, Kleeberger SR, 2009 Antiviral activity of Nrf2 in a murine model of respiratory syncytial virus disease. Am. J. Respir. Crit. Care Med 179, 138–150. [PubMed: 18931336]

Cho HY, Jedlicka AE, Gladwell W, Marzec J, McCaw ZR, Bienstock RJ, Kleeberger SR, 2015 Association of Nrf2 polymorphism haplotypes with acute lung injury phenotypes in inbred strains of mice. Antioxid. Redox Signal 22, 325–338. [PubMed: 25268541]

Cho HY, Jedlicka AE, Reddy SP, Kensler TW, Yamamoto M, Zhang LY, Kleeberger SR, 2002a Role of NRF2 in protection against hyperoxic lung injury in mice. Am. J. Resir. Cell Mol 26, 175–182.

Cho HY, Jedlicka AE, Reddy SP, Zhang LY, Kensler TW, Kleeberger SR, 2002b Linkage analysis of susceptibility to hyperoxia. Nrf2 is a candidate gene. Am. J. Resir. Cell Mol. Biol 26, 42–51.

Cho HY, and Kleeberger SR, 2015 Association of Nrf2 with airway pathogenesis: lessons learned from genetic mouse models. Arch. Toxicol 89, 1931–1957. [PubMed: 26194645]

Cho HY, Reddy SP, Debiase A, Yamamoto M, Kleeberger SR, 2005 Gene expression profiling of NRF2-mediated protection against oxidative injury. Free. Radic. Biol. Med 38, 325–343. [PubMed: 15629862]

Cho HY, van Houten B, Wang X, Miller-Degraff L, Fostel J, Gladwell W, Perrow L, Panduri V, Kobzik L, Yamamoto M, et al., 2012 Targeted Deletion of Nrf2 Impairs Lung Development and Oxidant Injury in Neonatal Mice. Antioxid. Redox Signal 17, 1066–1082. [PubMed: 22400915]

Clarke JD, Hsu A, Williams DE, Dashwood RH, Stevens JF, Yamamoto M, Ho E, 2011 Metabolism and Tissue Distribution of Sulforaphane in Nrf2 Knockout and Wild-Type Mice. Pharm. Res 28, 3171–3179. [PubMed: 21681606]

Clay Montier LL, Deng JJ, Bai Y, 2009 Number matters: control of mammalian mitochondrial DNA copy number. J. Genet. Genomics 36, 125–131. [PubMed: 19302968]

Dinkova-Kostova AT, Kostov RV, 2012 Glucosinolates and isothiocyanates in health and disease. Trends Mol. Med 18, 337–347. [PubMed: 22578879]

Egner PA, Chen JG, Zarth AT, Ng DK, Wang JB, Kensler KH, Jacobson LP, Munoz A, Johnson JL, Groopman JD, et al., 2014 Rapid and sustainable detoxication of airborne pollutants by broccoli sprout beverage: results of a randomized clinical trial in China. Cancer Prev. Res 7, 813–823.

Fahey JW, Holtzclaw WD, Wehage SL, Wade KL, Stephenson KK, Talalay P, 2015 Sulforaphane Bioavailability from Glucoraphanin-Rich Broccoli: Control by Active Endogenous Myrosinase. PLoS One 10, e0140963. [PubMed: 26524341]

Fahey JW, Wehage SL, Holtzclaw WD, Kensler TW, Egner PA, Shapiro TA, Talalay P, 2012 Protection of humans by plant glucosinolates: efficiency of conversion of glucosinolates to isothiocyanates by the gastrointestinal microflora. Cancer Prev. Res 5, 603–611.

Fahey JW, Zhang Y, Talalay P 1997, Broccoli sprouts: an exceptionally rich source of inducers of enzymes that protect against chemical carcinogens. Proc. Natl. Acad. Sci. U.S.A 94, 10367–10372. [PubMed: 9294217]

Furda A, Santos JH, Meyer JN, Van Houten B, 2014 Quantitative PCR-based measurement of nuclear and mitochondrial DNA damage and repair in mammalian cells. Methods Mol. Biol 1105, 419–437. [PubMed: 24623245]

Gasper AV, Al-Janobi A, Smith JA, Bacon JR, Fortun P, Atherton C, Taylor MA, Hawkey CJ, Barrett DA, Mithen RF, 2005 Glutathione S-transferase M1 polymorphism and metabolism of sulforaphane from standard and high-glucosinolate broccoli. Am. J. Clin. Nutr 82, 1283–1291. [PubMed: 16332662]

Harvey CJ, Thimmulappa RK, Sethi S, Kong X, Yarmus L, Brown RH, Feller-Kopman D, Wise R, Biswal S, 2011 Targeting Nrf2 signaling improves bacterial clearance by alveolar macrophages in patients with COPD and in a mouse model. Sci. Transl. Med 3, 78ra32.

Heber D, Li Z, Garcia-Lloret M, Wong AM, Lee TY, Thames G, Krak M, Zhang Y, Nel A, 2014 Sulforaphane-rich broccoli sprout extract attenuates nasal allergic response to diesel exhaust particles. Food Funct 5, 35–41. [PubMed: 24287881]

Hendrickson CM, Matthay MA, 2018 Endothelial biomarkers in human sepsis: pathogenesis and prognosis for ARDS. Pulm. Circ 8, 2045894018769876.

Holmstrom KM, Baird L, Zhang Y, Hargreaves I, Chalasani A, Land JM, Stanyer L, Yamamoto M, Dinkova-Kostova AT, Abramov AY, 2013 Nrf2 impacts cellular bioenergetics by controlling substrate availability for mitochondrial respiration. Biol. Open 2, 761–770. [PubMed: 23951401]

Islam MN, Das SR, Emin MT, Wei M, Sun L, Westphalen K, Rowlands DJ, Quadri SK, Bhattacharya S, Bhattacharya J, 2012 Mitochondrial transfer from bone-marrow-derived stromal cells to pulmonary alveoli protects against acute lung injury. Nature Med 18, 759–765. [PubMed: 22504485]

Kensler TW, Egner PA, Agyeman AS, Visvanathan K, Groopman JD, Chen JG, Chen TY, Fahey JW, Talalay P, 2013 Keap1-nrf2 signaling: a target for cancer prevention by sulforaphane. Top. Curr. Chem 329, 163–177. [PubMed: 22752583]

Kensler TW, Ng D, Carmella SG, Chen M, Jacobson LP, Munoz A, Egner PA, Chen JG, Qian GS, Chen TY, et al., 2012 Modulation of the metabolism of airborne pollutants by glucoraphanin-rich and sulforaphane-rich broccoli sprout beverages in Qidong, China. Carcinogenesis 33, 101–107. [PubMed: 22045030]

Kovac S, Angelova PR, Holmstrom KM, Zhang Y, Dinkova-Kostova AT, Abramov AY, 2015 Nrf2 regulates ROS production by mitochondria and NADPH oxidase. Biochim. Biophys. Acta 1850, 794–801. [PubMed: 25484314]

Kulkarni SR, Armstrong LE, Slitt AL, 2013 Caloric restriction-mediated induction of lipid metabolism gene expression in liver is enhanced by Keap1-knockdown. Pharm. Res 30, 2221–2231. [PubMed: 23884569]

Latte KP, Appel KE, Lampen A, 2011 Health benefits and possible risks of broccoli - an overview. Food Chem. Toxicol 49, 3287–3309. [PubMed: 21906651]

Li X, Michaeloudes C, Zhang Y, Wiegman CH, Adcock IM, Lian Q, Mak JCW, Bhavsar PK, Chung KF, 2018 Mesenchymal stem cells alleviate oxidative stress-induced mitochondrial dysfunction in the airways. J. Allergy Clin. Immunol 141, 1634–1645 e1635. [PubMed: 28911970]

Lopes RA, Neves KB, Tostes RC, Montezano AC, Touyz RM, 2015 Downregulation of Nuclear Factor Erythroid 2-Related Factor and Associated Antioxidant Genes Contributes to Redox-Sensitive Vascular Dysfunction in Hypertension. Hypertension 66, 1240–1250. [PubMed: 26503970]

Ludtmann MH, Angelova PR, Zhang Y, Abramov AY, Dinkova-Kostova AT, 2014 Nrf2 affects the efficiency of mitochondrial fatty acid oxidation. Biochem. J 457, 415–424. [PubMed: 24206218]

Marzec JM, Christie JD, Reddy SP, Jedlicka AE, Vuong H, Lanken PN, Aplenc R, Yamamoto T, Yamamoto M, Cho HY, et al., 2007 Functional polymorphisms in the transcription factor NRF2 in humans increase the risk of acute lung injury. FASEB J 21, 2237–2246. [PubMed: 17384144]

Matthay MA, Howard JP, 2012 Progress in modelling acute lung injury in a pre-clinical mouse model. Eur. Respir. J 39, 1062–1063. [PubMed: 22547731]

Matthay MA, Ware LB, Zimmerman GA, 2012 The acute respiratory distress syndrome. J. Clinic. Invest 122, 2731–2740.

Morrison TJ, Jackson MV, Cunningham EK, Kissenpfennig A, McAuley DF, O'Kane CM, Krasnodembskaya AD, 2017 Mesenchymal Stromal Cells Modulate Macrophages in Clinically Relevant Lung Injury Models by Extracellular Vesicle Mitochondrial Transfer. Am. J. Respir. Crit. Care Med 196, 1275–1286. [PubMed: 28598224]

Mouse EC, Stamatoyannopoulos JA, Snyder M, Hardison R, Ren B, Gingeras T, Gilbert DM, Groudine M, Bender M, Kaul R, et al., 2012 An encyclopedia of mouse DNA elements (Mouse ENCODE). Genome Biol 13, 418. [PubMed: 22889292]

Perera RM, Stoykova S, Nicolay BN, Ross KN, Fitamant J, Boukhali M, Lengrand J, Deshpande V, Selig MK, Ferrone CR, et al., 2015 Transcriptional control of autophagy-lysosome function drives pancreatic cancer metabolism. Nature 524, 361–365. [PubMed: 26168401]

Sakurai H, Morishima Y, Ishii Y, Yoshida K, Nakajima M, Tsunoda Y, Hayashi SY, Kiwamoto T, Matsuno Y, Kawaguchi M, et al., 2018 Sulforaphane ameliorates steroid insensitivity through an

Nrf2-dependent pathway in cigarette smoke-exposed asthmatic mice. Free. Radic. Biol. Med 129, 473–485. [PubMed: 30312763]

Sestili P, Paolillo M, Lenzi M, Colombo E, Vallorani L, Casadei L, Martinelli C, Fimognari C, 2010 Sulforaphane induces DNA single strand breaks in cultured human cells. Mut. Res 689, 65–73. [PubMed: 20510253]

Strauss KA, DuBiner L, Simon M, Zaragoza M, Sengupta PP, Li P, Narula N, Dreike S, Platt J, Procaccio V, et al., 2013 Severity of cardiomyopathy associated with adenine nucleotide translocator-1 deficiency correlates with mtDNA haplogroup. Proc. Natl. Acad. Sci. U.S.A 110, 3453–3458. [PubMed: 23401503]

Strom J, Xu B, Tian X, Chen QM, 2016 Nrf2 protects mitochondrial decay by oxidative stress. FASEB J 30, 66–80. [PubMed: 26340923]

Sutendra G, Michelakis ED, 2014 The metabolic basis of pulmonary arterial hypertension. Cell Metab 19, 558–573. [PubMed: 24508506]

Tatarenkov A, Avise JC, 2007 Rapid concerted evolution in animal mitochondrial DNA. Proc. Biol. Sci 274, 1795–1798. [PubMed: 17490947]

Tebay LE, Robertson H, Durant ST, Vitale SR, Penning TM, Dinkova-Kostova AT, Hayes JD, 2015 Mechanisms of activation of the transcription factor Nrf2 by redox stressors, nutrient cues, and energy status and the pathways through which it attenuates degenerative disease. Free. Radic. Biol. Med 88, 108–146. [PubMed: 26122708]

Wise RA, Holbrook JT, Criner G, Sethi S, Rayapudi S, Sudini KR, Sugar EA, Burke A, Thimmulappa R, Singh A, et al., 2016 Lack of Effect of Oral Sulforaphane Administration on Nrf2 Expression in COPD: A Randomized, Double-Blind, Placebo Controlled Trial. PLoS One 11, e0163716. [PubMed: 27832073]

Yanaka A, Fahey JW, Fukumoto A, Nakayama M, Inoue S, Zhang S, Tauchi M, Suzuki H, Hyodo I, Yamamoto M, 2009 Dietary sulforaphane-rich broccoli sprouts reduce colonization and attenuate gastritis in Helicobacter pylori-infected mice and humans. Cancer Prev. Res 2, 353–360.

Yue F, Cheng Y, Breschi A, Vierstra J, Wu W, Ryba T, Sandstrom R, Ma Z, Davis C, Pope BD, et al., 2014 A comparative encyclopedia of DNA elements in the mouse genome. Nature 515, 355–364. [PubMed: 25409824]

Yue P, Yang X, Ning P, Xi X, Yu H, Feng Y, Shao R, Meng X, 2018 A mitochondria-targeted ratiometric two-photon fluorescent probe for detecting intracellular cysteine and homocysteine. Talanta 178, 24–30. [PubMed: 29136818]

Zheng Y, Tao S, Lian F, Chau BT, Chen J, Sun G, Fang D, Lantz RC, Zhang DD, 2012 Sulforaphane prevents pulmonary damage in response to inhaled arsenic by activating the Nrf2-defense response. Toxicol. Appl. Pharmacol 265, 292–299. [PubMed: 22975029]

HIGHLIGHTS

- Sulforaphane prevented murine acute lung injury in an Nrf2-dependent manner.
- Pulmonary sulforaphane activity was featured by linking mitochondria and Nrf2.
- Potential ARE motifs were enriched in sulforaphane-induced energy metabolism genes.
- Enhanced mitochondrial biogenesis conveyed airway defense against oxidant disorders.

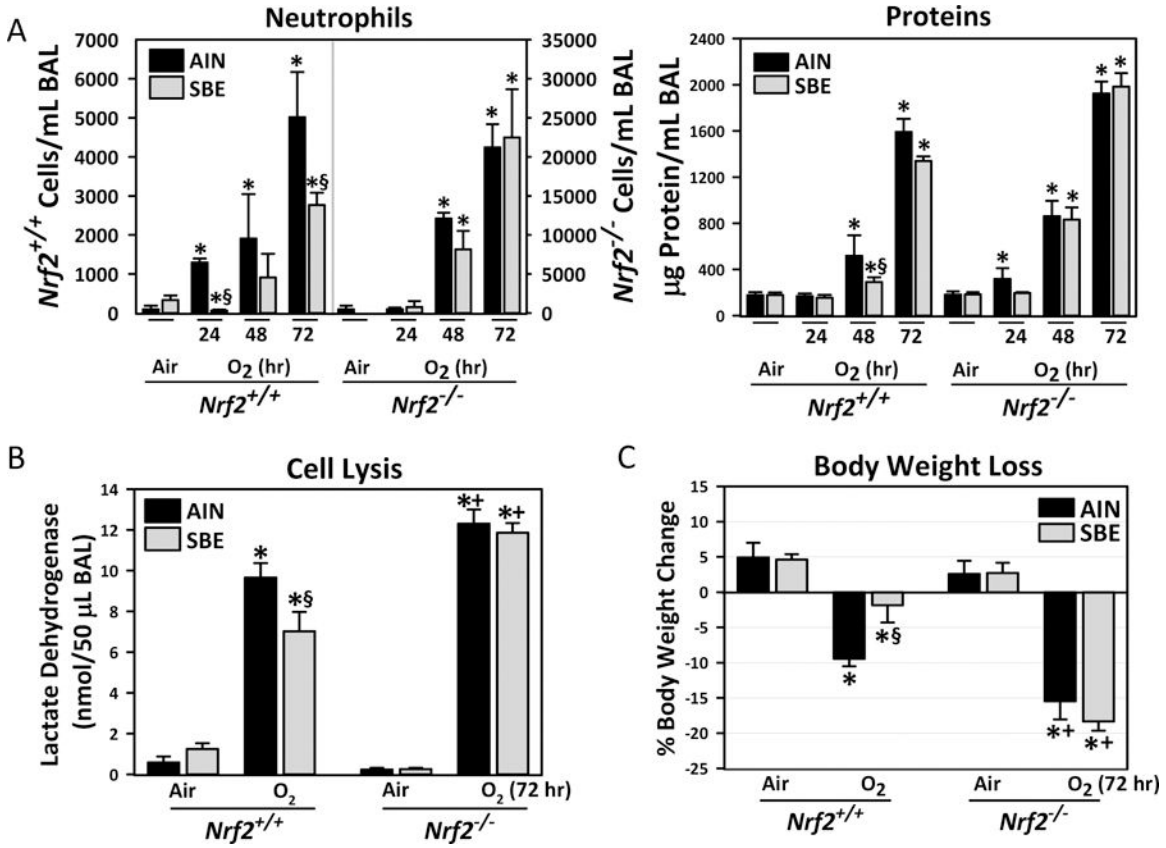

Fig. 1. Nrf2-dependent protective effect of dietary glucoraphanin (SBE) on hyperoxia (O_2)-induced lung injury.

(A) Bronchoalveolar lavage (BAL) fluid analysis determined numbers of neutrophils for inflammation and total protein concentration for vascular permeability (n = 3/group for air and 48 h O_2, n = 6/group for 72h O_2), and (B) activity of lactate dehydrogenase (LDH) for cytotoxicity (n = 3/group for air, n = 4–5/group for O_2). (C) Hyperoxia susceptibility determined by body weight loss was indicated as percent body weight change at the end of 72 h hyperoxia or air exposure (day 18) compared to the onset of the diet (day 1, n = 3/group for air, n = 6/group for O_2). Data presented as group mean±SE. Two-way ANOVA used for all statistical analyses. *, $P < 0.05$ vs. genotype- and diet-matched air controls. +, $P < 0.05$ vs. diet- and exposure-matched *Nrf2*$^{+/+}$ mice. §, $P < 0.05$ vs genotype- and exposure-matched AIN group.

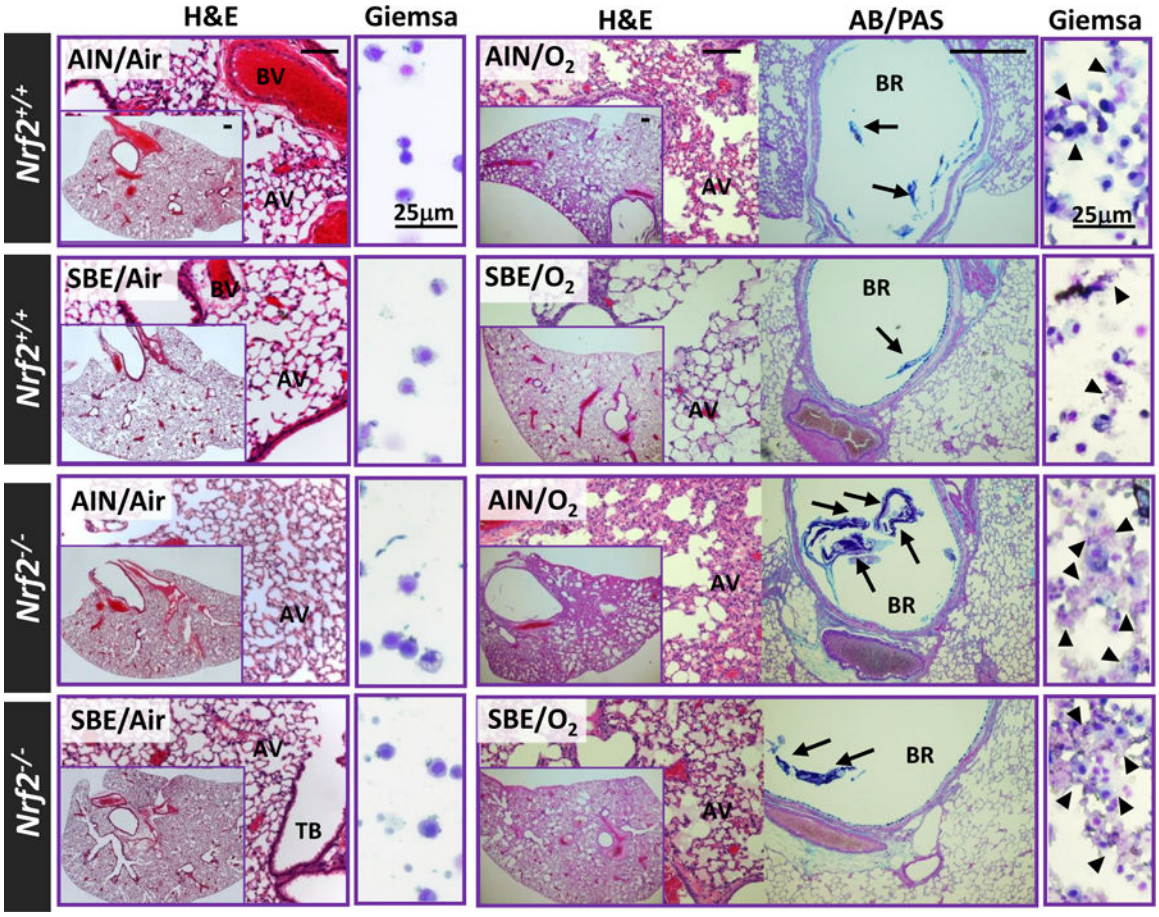

Fig. 2. Nrf2-dependent mitigation of hyperoxia (O_2)-induced pulmonary histopathology by dietary glucoraphanin (SBE).

Representative light photomicrographs of lung tissue sections stained with H&E and AB/PAS or cytocentrifuged BAL cells stained with Giemsa after 14 days of normal (AIN) or standardized broccoli extract-containing diet (SBE) followed by 72 h exposure to normoxia (room air) or O_2. AV, alveoli; BR, bronchi; BV, blood vessel; TB, terminal bronchiole. Arrows=secreted mucus stained. Arrow heads=lysed cells. Bars (unlabeled) = 100 μm.

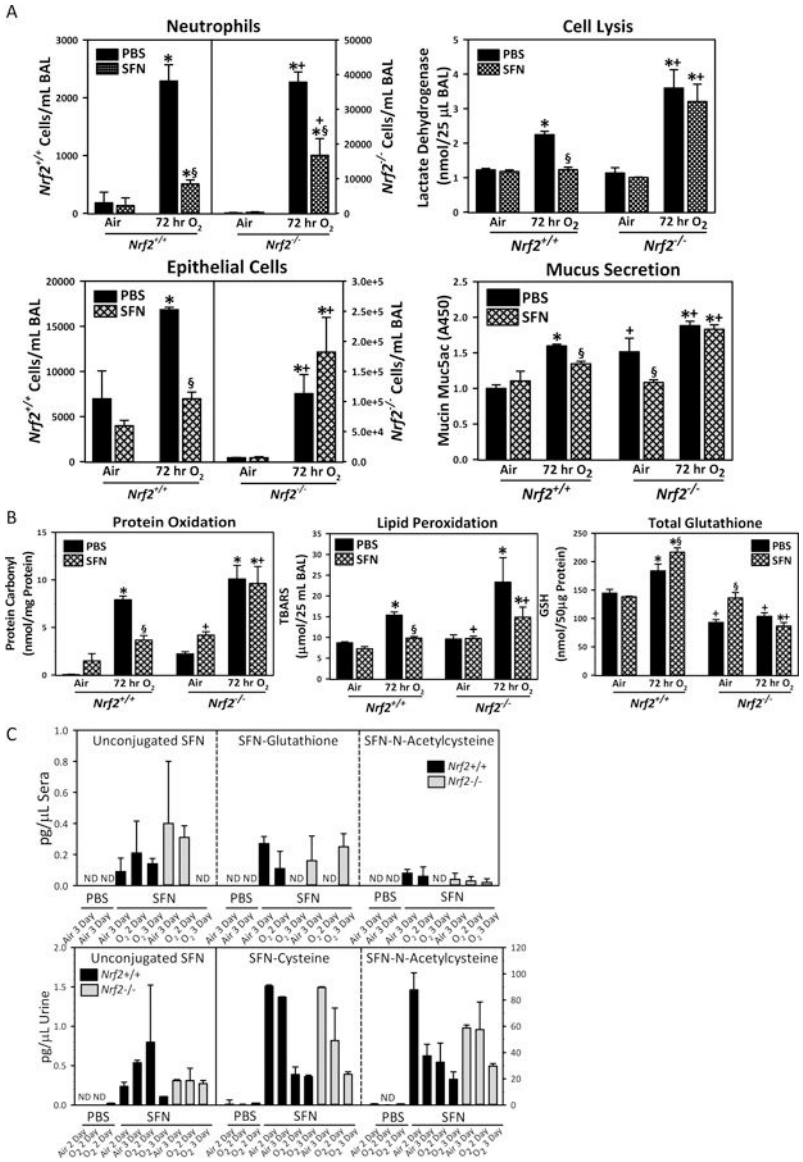

Fig. 3. Nrf2-dependent protective effect of oral sulforaphane (SFN) on hyperoxia (O_2)-induced lung injury.

(A) Bronchoalveolar lavage (BAL) fluids were analyzed for the numbers of lung epithelial cells and neutrophils (n = 3/group for air, n = 6/group for O_2), activity of lactate dehydrogenase (n = 3/group for air, n = 4/group for O_2), and the amount of secreted mucin proteins (Muc5AC, n = 3/group for air, n = 5/group for O_2). (B) Lung oxidative stress indicated as oxidized protein (protein carbonyl), lipid peroxidation (thiobarbituric acid reactive substances, TBARS) in BAL, and total glutathione (GSH) levels in lung homogenates. Data presented as mean ± SE (n = 3/group). Two-way ANOVA used for all statistical analyses. *, $P < 0.05$ vs. genotype- and pretreatment-matched air controls. +, $P < 0.05$ vs. pretreatment- and exposure-matched *Nrf2*$^{+/+}$ mice. §, $P < 0.05$ vs. genotype- and exposure-matched PBS. (C) Major SFN metabolites including SFN-glutathione (GSH), SFN-cysteine, and SFN-N-acetylcysteine (NAC) as well as non-metabolized (unconjugated) SFN were determined in aliquots of diluted urine or deproteinated sera at 2 or 3 days after

air or O_2 exposure following oral dose of PBS or SFN by HPLC-mass spectrometry. Data presented as mean ± SE (n=3/group). ND=not detected.

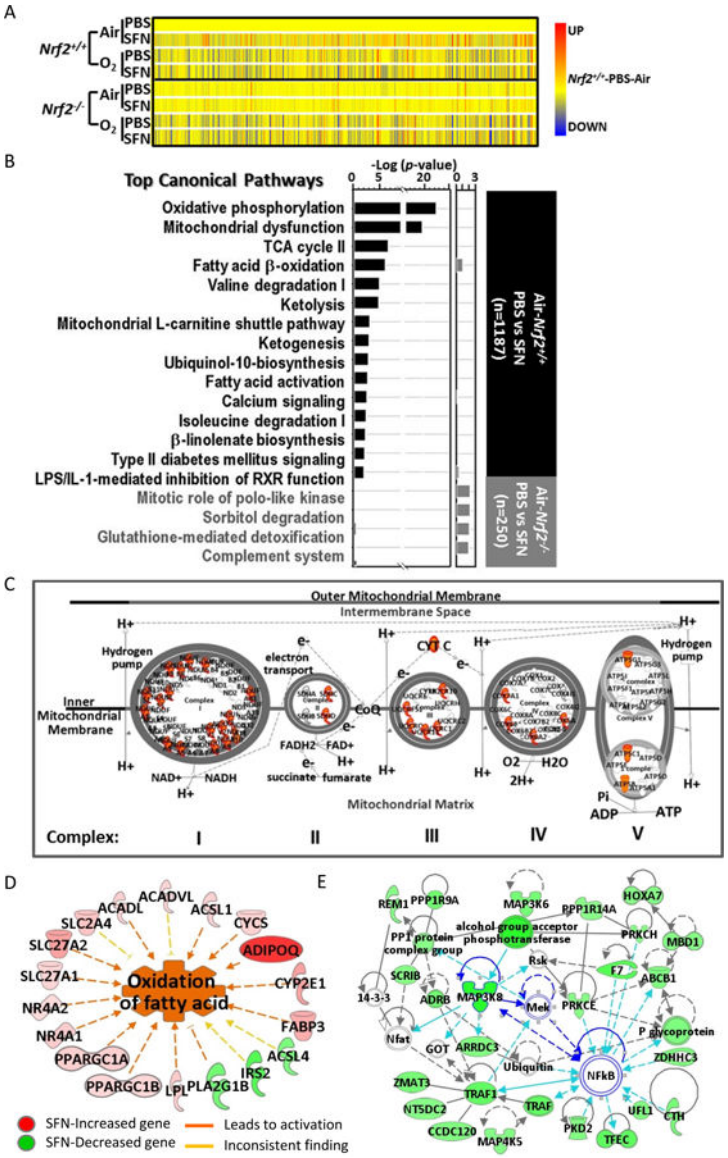

Fig. 4. Nrf2-dependent changes of basal lung transcriptome by sulforaphane (SFN) pretreatment.

(A) Heat map from hierarchical clustering analysis depicts expression profiles of SFN-responded genes in *Nrf2*$^{+/+}$ after 72 h hyperoxia (O_2) exposure (n = 1,187, $P < 0.01$ with moderated t-test). Heat map for the same genes in *Nrf2*$^{-/-}$ mice were shown for comparison. Color bar indicates average expression intensity (n = 3/group) normalized to *Nrf2*$^{+/+}$-PBS-Air group. (B) Top canonical pathways of lung genes significantly altered by SFN in air-exposed *Nrf2*$^{+/+}$ (black bars) and in air-exposed *Nrf2*$^{-/-}$ mice (grey bars). (C) Mitochondrial oxidative phosphorylation complex is illustrated with genes (in red) that were induced by SFN treatment in *Nrf2*$^{+/+}$ mice exposed to normoxia (room air). (D) Top diseases and bio-functions of SFN-responsive lung genes in *Nrf2*$^{+/+}$ mice included energy metabolism such as fatty acid beta-oxidation. (E) Lung genes significantly reduced by SFN in *Nrf2*$^{+/+}$ mice were involved in the network of organismal injury and abnormality (scores 32–41), in which key molecules such as TNF receptor associated factor 1 (*Traf1*) and multiple mitogen-

activated protein kinase (MAPK) cascade enzymes (e.g., *Map3k8*) were predicted to play central roles with NF-κB. Analysis was done by Ingenuity Pathway Analysis software.

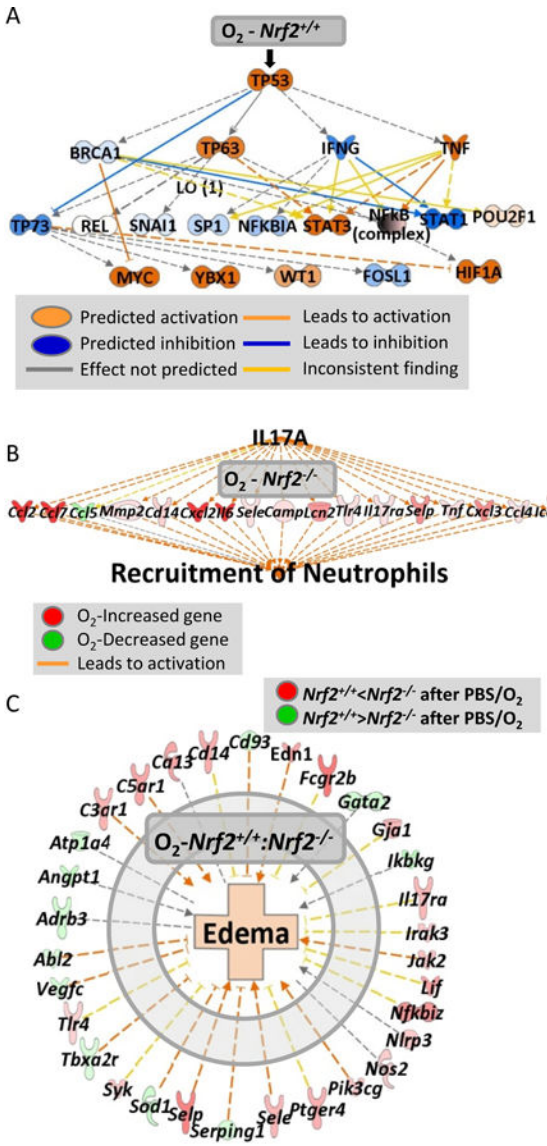

Fig. 5. Nrf2-dependent lung transcriptome changes by hyperoxia (O_2).

(A) Pathway analysis for hyperoxia-responsive genes in PBS-received *Nrf2*$^{+/+}$ mice (n= 7162 genes, $P < 0.01$, Moderated t-test) demonstrated p53 as a key upstream regulator for the hyperoxia-altered lung genes, which may sequentially modulate other signal transducers. (B) In *Nrf2*$^{-/-}$ mice that received PBS, O_2 altered genes (n = 4,799, $P < 0.01$) involved predominantly in IL-17A signaling pathway, which may lead to severe neutrophil infiltration. (C) Nrf2-dependently modulated genes during hyperoxia (n = 816, $P < 0.01$) such as *Selp* and *Fcgr2b* may contribute to the differential lung edema between *Nrf2*$^{+/+}$ and *Nrf2*$^{-/-}$ mice given PBS.

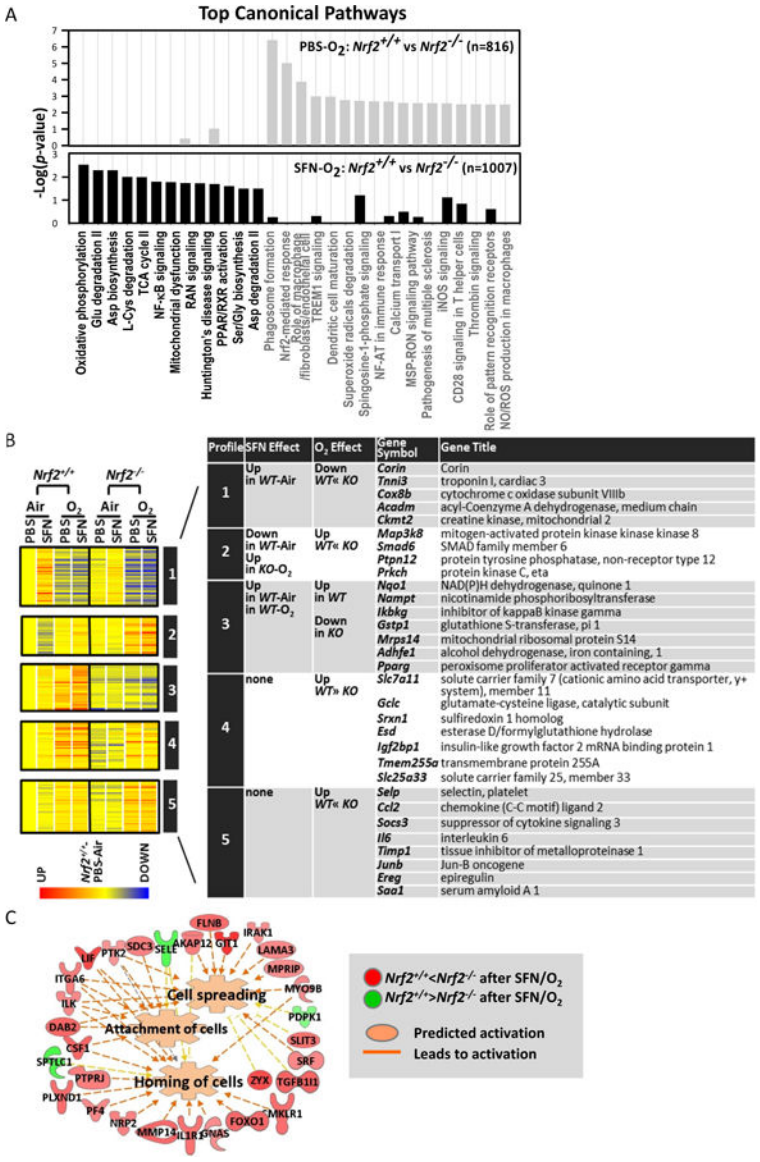

Profile	SFN Effect	O_2 Effect	Gene Symbol	Gene Title
1	Up in *WT*-Air	Down *WT*« *KO*	*Corin*	Corin
			Tnni3	troponin I, cardiac 3
			Cox8b	cytochrome c oxidase subunit VIIIb
			Acadm	acyl-Coenzyme A dehydrogenase, medium chain
			Ckmt2	creatine kinase, mitochondrial 2
2	Down in *WT*-Air Up in *KO*-O_2	Up *WT*« *KO*	*Map3k8*	mitogen-activated protein kinase kinase kinase 8
			Smad6	SMAD family member 6
			Ptpn12	protein tyrosine phosphatase, non-receptor type 12
			Prkch	protein kinase C, eta
3	Up in *WT*-Air in *WT*-O_2	Up in *WT* Down in *KO*	*Nqo1*	NAD(P)H dehydrogenase, quinone 1
			Nampt	nicotinamide phosphoribosyltransferase
			Ikbkg	inhibitor of kappaB kinase gamma
			Gstp1	glutathione S-transferase, pi 1
			Mrps14	mitochondrial ribosomal protein S14
			Adhfe1	alcohol dehydrogenase, iron containing, 1
			Pparg	peroxisome proliferator activated receptor gamma
4	none	Up *WT*» *KO*	*Slc7a11*	solute carrier family 7 (cationic amino acid transporter, y+ system), member 11
			Gclc	glutamate-cysteine ligase, catalytic subunit
			Srxn1	sulfiredoxin 1 homolog
			Esd	esterase D/formylglutathione hydrolase
			Igf2bp1	insulin-like growth factor 2 mRNA binding protein 1
			Tmem255a	transmembrane protein 255A
			Slc25a33	solute carrier family 25, member 33
5	none	Up *WT*« *KO*	*Selp*	selectin, platelet
			Ccl2	chemokine (C-C motif) ligand 2
			Socs3	suppressor of cytokine signaling 3
			Il6	interleukin 6
			Timp1	tissue inhibitor of metalloproteinase 1
			Junb	Jun-B oncogene
			Ereg	epiregulin
			Saa1	serum amyloid A 1

Fig. 6. Nrf2-dependent lung transcriptome changes by sulforaphane (SFN) pretreatment during hyperoxia (O_2) exposure.

(A) Top canonical pathways of Nrf2-dependently changed gene transcripts with PBS (top, gray bars) or SFN (bottom, black bars) pretreatment in response to hyperoxia. (B) Profile analysis classified Nrf2-dependently regulated genes by similar expression patterns. (C) Pathway analysis for SFN-responsive genes in hyperoxia-exposed *Nrf2*$^{-/-}$ mice (n= 533, $P <$ 0.01) depicted that genes altered by SFN only in these mice (e.g., *Sele*, *Itga5*, *Lif*, *Flnb*) may stimulate cellular movement and interaction by activating cell spreading, attachment, and homing, through which SFN may exert Nrf2-independent responses against hyperoxia in *Nrf2*$^{-/-}$ mice. Analyses were done using Ingenuity Pathway Analysis and GeneSpring software.

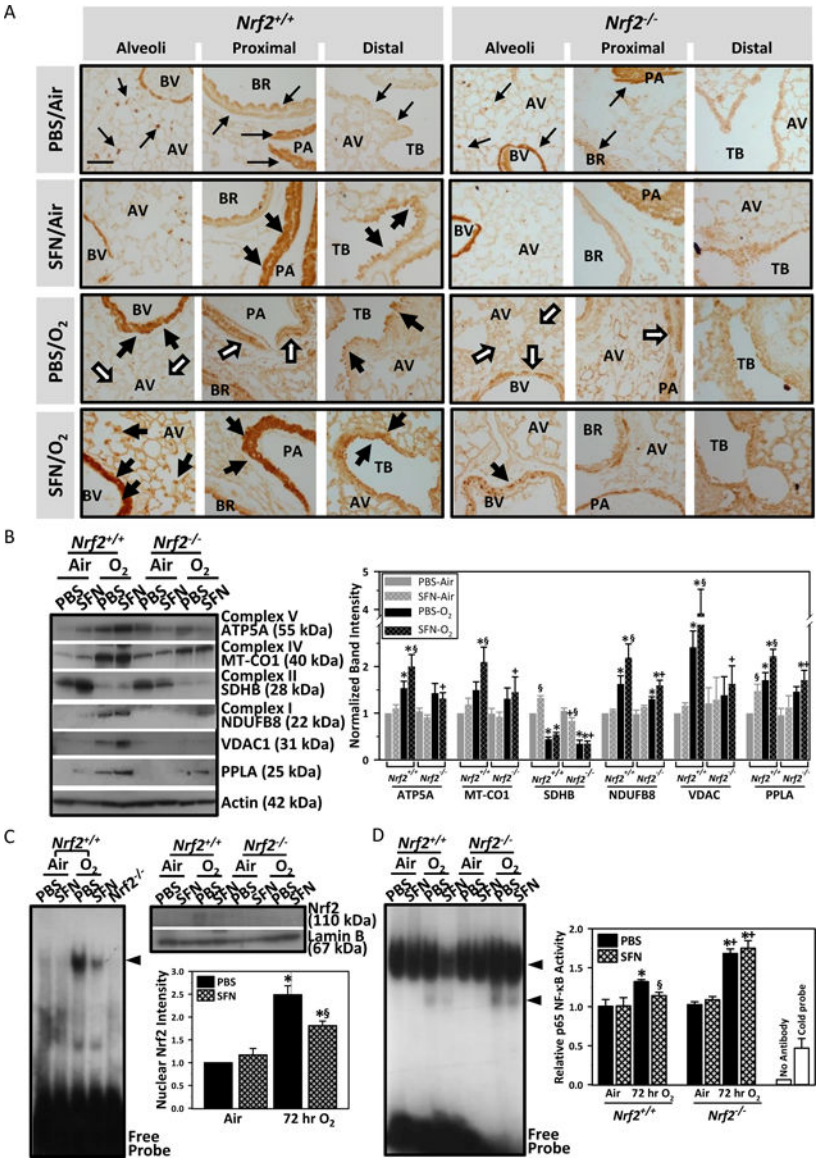

Fig. 7. Validation of lung gene expression array analysis.

(A) Immunohistochemical localization of voltage-dependent anion-selective channel 1 (VDAC1)/porin, a mitochondrial membrane potential marker, in lung tissue sections. Brown dots indicate VDAC1-positive cells. Representative light photomicrographs are shown (n = 3–4/group). VDAC1 localization at baseline lung (PBS/Air) is indicated by small arrows. Thick black arrows indicate areas with increased VDAC1 expression compared to genotype-matched PBS/Air. White arrows indicate areas with decreased VDAC1 compared to genotype-matched PBS/Air. SFN = sulforaphane. O_2 = Hyperoxia. AV, alveoli; BR, bronchi; BV, blood vessel; PA, pulmonary artery; TB, terminal bronchiole. Bar = 100 μm. (B) Aliquots of lung cytosolic proteins were subjected for Western blotting using specific antibodies. Representative images from multiple analyses of pooled proteins (n = 3/antibody) presented. ATP5A = ATP synthase subunit alpha, mitochondrial. MT-CO1 = mitochondrially encoded cytochrome c oxidase subunit 1. SDH8 = succinate dehydrogenase

subunit B. NDUFB8 = NADH dehydrogenase (Ubiquinone) 1 beta subcomplex, 8. VDAC1 = Voltage-dependent anion-selective channel 1. PPLA=Cardiac phospholamban. kDa = kilodalton. Scanned band images were quantitated by densitometry. Data presented as group mean ± SE. Two-way ANOVA used for all statistical analyses. *, $P < 0.05$ vs. genotype- and pretreatment-matched air controls. +, $P < 0.05$ vs. pretreatment- and exposure-matched *Nrf2*$^{+/+}$ mice. §, $P < 0.05$ vs. genotype- and exposure-matched PBS group. (C) Aliquots of pooled lung nuclear protein (5 μg) were incubated with an end-labeled oligonucleotide probe containing antioxidant response element (ARE) consensus sequence, and gel shift analysis determined total ARE binding. Nuclear proteins (5 μg) from PBS/hyperoxia-*Nrf2*$^{-/-}$ mice were run as a negative control. Nuclear proteins were subjected for Western blot analysis using Nrf2-specific antibody and images were quantified. *, $P < 0.05$ vs. pretreatment-matched air controls. §, $P < 0.05$ vs. PBS/hyperoxia group. (D) Aliquots of pooled lung nuclear protein (5 μg) were incubated with an end-labeled oligonucleotide probe containing NF-κB consensus sequence, and gel shift analysis determined total NF-κB binding. Two shifted bands (arrow heads) indicate total DNA-NF-κB complex. Specific activity for p65 NF-κB subunit was quantified using a transcription factor ELISA. Nuclear proteins from PBS/hyperoxia-*Nrf2*$^{-/-}$ mice were used for reaction with cold probes (20 pmol addition of oligonucleotide) and for no antibody control to verify the reaction specificity. *, $P < 0.05$ vs. genotype- and pretreatment-matched air controls. +, $P < 0.05$ vs. pretreament- and exposure-matched *Nrf2*$^{+/+}$ mice. §, $P < 0.05$ vs. genotype- and exposure-matched PBS group.

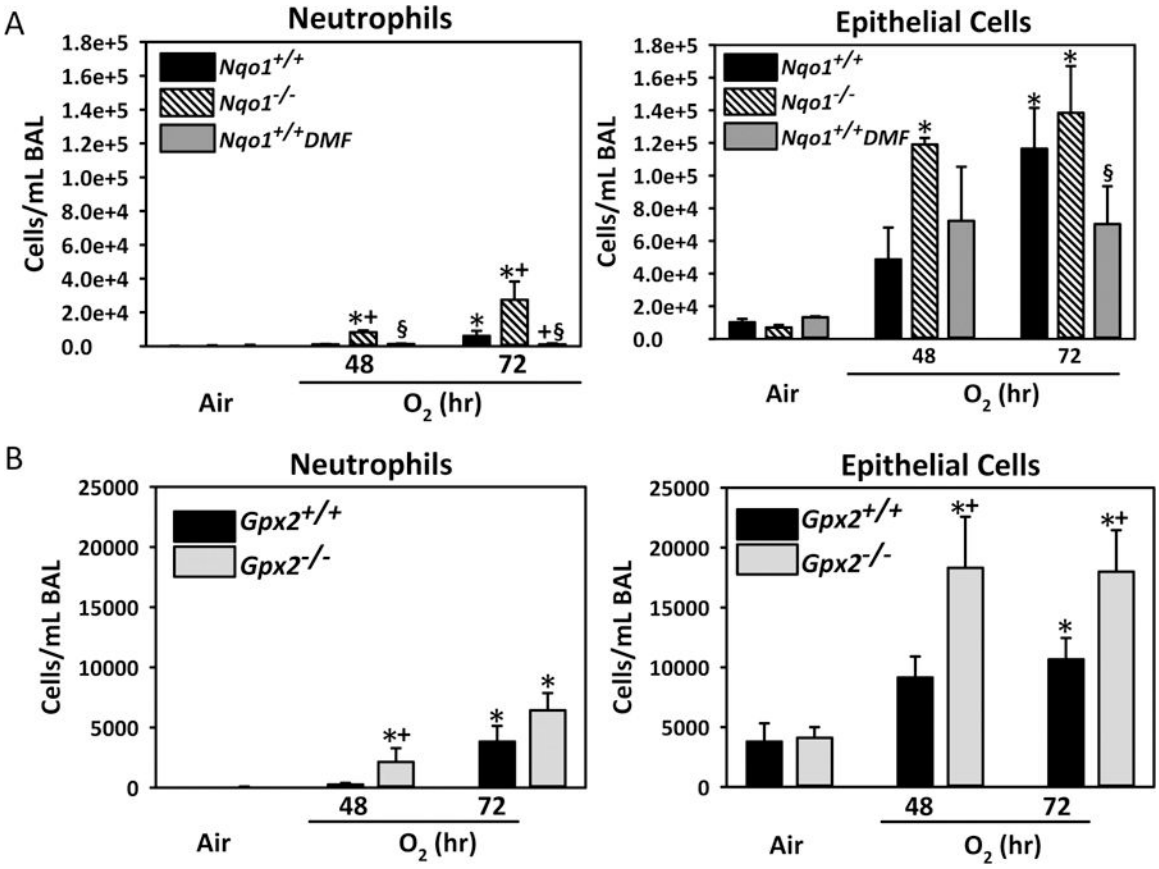

Fig. 8. Role of Sulforaphane-responsive antioxidant enzymes in hyperoxia-induced lung injury

(A) Numbers of neutrophils and epithelial cells found in bronchopulmonary lavage (BAL) fluid from wild-type (*Nqo1*$^{+/+}$), dimethyl fumarate (DMF)-fed wild-type (*Nqo1*$^{+/+}$*DMF*), and *Nqo1*$^{-/-}$ mice after exposure to air and O_2 (48–72 h). Data presented as group mean ± SE (n = 3/group for air, n = 5/group for 48 h O_2, n = 7/group for 72 h O_2). (B). Numbers of neutrophils and epithelial cells found in BAL fluid from *Gpx2*$^{+/+}$ and *Gpx2*$^{-/-}$ mice after exposure to air and O_2 (48–72 h). Data presented as group mean ± SE (n = 3/group for air, n = 6/group for 48 h O_2, n = 10/group for 72 h O_2). Two-way ANOVA used for statistical analyses. *, $P < 0.05$ vs. genotype and air controls. +, $P < 0.05$ vs. exposure-matched wild-type mice. §, $P < 0.05$ vs. exposure-matched *Nqo1*$^{-/-}$ mice.

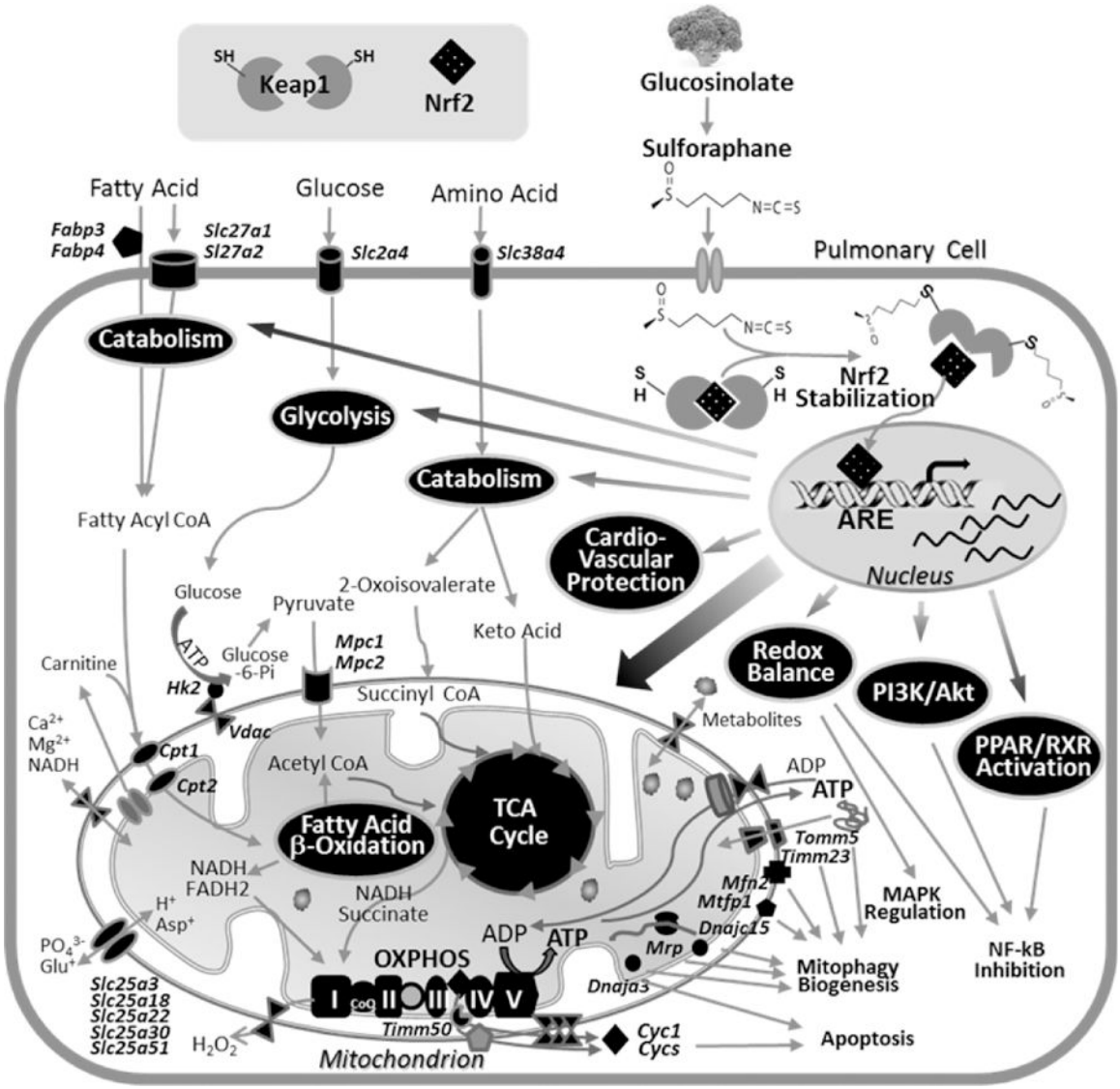

Fig. 9. Potential mechanisms of Nrf2-dependent sulforaphane action in lung protection.

Dietary sulforaphane is known to stabilize cytoplasmic Nrf2 through Keap1 binding to inhibit Nrf2 ubiquitination for its proteasomal degradation. Stabilized Nrf2 may exert transcriptional activation of antioxidant response element (ARE)-responsive genes involved in redox regulation but also in fatty acid, glucose, and amino acid catabolism including enzymes and cellular transporters. Transcription activation then results in provision of metabolic substrates for mitochondrial machinery, tricarboxylic acid (TCA) cycle, fatty acid β-oxidation (FAO), and oxidative phosphorylation (OXPHOS) complex as well as mitochondrial symporters and transporters. Nrf2 may also directly upregulate ARE-bearing genes that encode these mitochondrial apparatus and mitochondrial quality control processes (i.e., mitophagy, biogenesis). Enhanced cyctochrome C (Cyc1) from OXPHOS is known to cause apoptosis, and ARE-responsive vasodilation and cardioprotective genes may protect pulmonary hypertension and vascular remodeling. Overall, sulforaphane-Nrf2 responses enrich mitochondrial bioenergetics to produce ATP on cellular demand but also facilitate

other mitochondrial functions for cellular homeostasis against oxidative stress. Pathway analyses indicated that these Nrf2-dependently regulated lung genes are associated with pathways including peroxisome proliferator-activated receptor/retinoid X receptor (PPAR/RXR) activation, phosphatidylinositol 3- kinase (PI3K)/Akt signaling, which may modulate NF-κB and MAPK signaling cascade. Proteins and cellular processes predicted to be modulated by SFN-Nrf2 axis are highlighted in black.

Table 1.

Representative lung genes induced by sulforaphane and potential antioxidant response elements (AREs).

Category	RefSeq ID	†FI	Gene Symbol	Gene Title	Functions	‡Potential AREs No: PWM
Mitochondrial Function & Energy Metabolism	NM_009605	8.72	***Adipoq*** *	adiponectin, C1Q and collagen domain containing	fat metabolism, glucose uptake and insulin sensitivity	10: 6.9–10.6
	NM_024406	4.89	***Fabp4***	fatty acid binding protein 4, adipocyte	long chain fatty acid/ retinoic acid delivery	10: 6.4–15.6
	NM_146050	4.01	***Oit1***	oncoprotein induced transcript 1	negative regulation of insulin secretion	19: 6.4–13.5
	NM_011978	3.50	***Slc27a2***	solute carrier family 27 (fatty acid transporter), member 2	very long-chain fatty acid transporter	14: 6.5–11.5
	NM_009204	2.18	***Slc2a4***	solute carrier family 2 (facilitated glucose transporter), member 4	glucose transmembrane transporter (uptake), GLUT4	4: 7.9–9.5
	NM_007381	1.75	***Acadl*** *	acyl-Coenzyme A dehydrogenase, long-chain	fatty acid β-oxidation	15: 6.8–14.2
	NM_009949	1.52	***Cpt2*** *	carnitine palmitoyltransferase 2	fatty acid β-oxidation	9: 6.8–15.0
	NM_146108	1.44	***Hibadh***	3-hydroxyisobutyryl-coenzyme A hydrolase	amino acid catabolic process	6: 6.6–14.7
	NM_011099	1.23	***Pkm2*** *	pyruvate kinase, muscle	glycolysis	10: 6.8–15.1
	NM_009944	4.05	***Cox7a1***	cytochrome c oxidase, subunit VIIa 1	mt OXPHOS	11: 6.9–14.2
	NM_001161419	1.83	***Atp5g1*** *	ATP synthase, H+ transporting, mitochondrial F0 complex, subunit c1 (subunit 9)	mt OXPHOS	9: 7.0–14.1
	NM_008904	1.76	***Ppargc1a***	peroxisome proliferative activated receptor, gamma, coactivator 1 alpha	mt biogenesis	8: 6.6–9.5
	NM_025567	1.68	***Cyc1***	cytochrome c-1	mt OXPHOS	7: 7.1–12.0
	NM_001160038	1.63	***Ndufs1*** *	NADH dehydrogenase (ubiquinone) Fe-S protein 1	mt OXPHOS	11: 6.4–11.0
	NM_026452	1.62	***Coq9*** *	coenzyme Q9 homolog (yeast)	mt OXPHOS	10: 6.6–17.4
	NM_023374	1.58	***Sdhb*** *	succinate dehydrogenase complex, subunit B, iron sulfur	mt OXPHOS	12: 7.2–10.6
	NM_025710	1.57	***Uqcrfs1***	ubiquinol-cytochrome c reductase, Rieske iron-sulfur polypeptide 1	mt OXPHOS	6: 6.7–12.8
	NM_029573	1.55	***Idh3a*** *	isocitrate dehydrogenase 3 (NAD+) alpha	mt TCA cycle	12: 6.5–14.9
	NM_133201	1.41	***Mfn2***	mitofusin 2	mt fusion	4: 7.8–11.2
	NM_018819	1.41	***Mpc1*** *	mitochondrial pyruvate carrier 1	mt pyruvate transporter	11: 6.4–16.5
Cardio-vascular Tone & Muscular Function	NM_008725	31.74	***Nppa***	natriuretic peptide type A	blood pressure	14: 6.4–11.8
	NM_001141927	10.12	***Pln***	phospholamban	Ca^{2+} homeostasis	9: 6.6–14.8
	NM_001122756	7.76	***Corin*** *	corin	blood pressure	12: 6.6–17.2
	NM_009406	6.94	***Tnni3***	troponin I, cardiac 3	Ca^{2+} homeostasis	9: 7.1–12.0
	NM_010859	5.90	***Myl3***	myosin, light polypeptide 3	cardiac muscle contraction	10: 6.8–14.1
Antioxidant & Defense	NM_008522	13.07	***Ltf***	lactotransferrin	anti-microbial	7: 7.0–11.8
	NM_028801	5.74	***Muc5b***	mucin 5, subtype B, tracheobronchial	mucosal defense	9: 6.5–14.6
	NM_029803	5.06	***Ifi27l2a***	interferon, alpha-inducible protein 27 like 2A	adipocytokine, mt biogenesis	7: 7.2–11.4
	NM_016771	4.76	***Sult1d1***	sulfotransferase family 1D, member 1	metabolic process	7: 8.1–10.4
	NM_007940	4.36	***Ephx2***	epoxide hydrolase 2, cytoplasmic	lipid phosphatase	10: 6.9–12.6

Category	RefSeq ID	†FI	Gene Symbol	Gene Title	Functions	‡Potential AREs No: PWM
	NM_007606	4.08	***Car3***	carbonic anhydrase 3	antioxidant, muscle	14: 6.7–13.1
	NM_026183	4.02	***Slc47a1***	solute carrier family 47, member 1	multidrug and toxic compound transporters	9: 6.5–13.3
	NM_010362	2.21	***Gsto1*** *	glutathione S-transferase omega 1	L-ascorbic acid biosynthesis	9: 7.8–13.7
	NM_007452	1.34	***Prdx3*** *	peroxiredoxin 3	antioxidant, mt	11: 6.6–10.9

mt, mitochondria. OXPHOS, oxidative phosphorylation. PWM, position weight matrix. ARE, antioxidant response element.

*Genes with ChIP-Seq data published by the Encyclopedia of Mouse DNA Elements Consortium (Mouse et al., 2012; Yue et al., 2014).

†Fold increase in SFN/air vs. PBS/air in *Nrf2*$^{+/+}$ mice.

‡Number of potential AREs and their PWM range. Expanded data for full gene list and ARE search in Supplementary Tables E1 and E3.

Table 2.

Mitochondrial genome copy numbers determined by droplet digital PCR (ddPCR).

	Nrf2$^{+/+}$		*Nrf2*$^{-/-}$	
Pre-treatment	**PBS**	**SFN**	**PBS**	**SFN**
Air	148.81 ± 10.53	255.31 ± 44.73	175.38 ± 17.39	190.78 ± 12.04
Hyperoxia (72 h)	168.48 ± 39.99	223.43 ± 27.10	141.54 ± 24.95	172.36 ± 51.76

Mitochondria copy number determined by comparing the abundance of mitochondrial DNA to nuclear DNA in 1 ng total DNA. Mean ± SE presented (n=3/group). SFN=sulforaphane.